In Silico Screening Study for the Identification of Potential Tankyrase 1 Inhibitors against Ovarian Cancer

By

Gazi Taznur Islam
22146056
Anima Rahman Anu
22146085

A thesis submitted to the School of Pharmacy in partial fulfillment of the requirements for the degree of Bachelor of Pharmacy (B. Pharm. Hons.)

School of Pharmacy
BRAC University
June, 2026

Declaration

It is hereby declared that

1. The thesis submitted is our own original work while completing a degree at BRAC University.
2. The thesis does not contain material previously published or written by a third party, except where this is appropriately cited through full and accurate referencing.
3. The thesis does not contain material which has been accepted, or submitted, for any other degree or diploma at a university or other institution.
4. We have acknowledged all main sources of help.

Student's Full Name & Signature:

Gazi Taznur Islam	**Anima Rahman Anu**
22146056	22146085

Approval

The project titled "*In silico* Screening Study for the Identification of Potential Tankyrase 1 Inhibitors against Ovarian Cancer" submitted by

1. Gazi Taznur Islam (22146056)
2. Anima Rahman Anu (22146085)

of Summer, 2025 has been accepted as satisfactory in partial fulfillment of the requirement for the degree of Bachelor of Pharmacy (B. Pharm. Hons.).

Examining Committee:

Supervisor:
(Member)

_____

Namara Mariam Chowdhury
Senior Lecturer, School of Pharmacy
BRAC University

Program Coordinator:
(Member)

_____

Namara Mariam Chowdhury
Senior Lecturer, School of Pharmacy
BRAC University

Departmental Head:
(Chair)

_____

Sharmind Neelotpol, PhD
Professor, School of Pharmacy
BRAC University

Ethics Statement

This project does not involve any kind of animal or human trial.

Abstract

Ovarian cancer remains one of the leading causes of cancer-related mortality among women, highlighting the need for developing effective therapeutic strategies. The tankyrase 1 (TNKS1), a key regulator of Wnt/β-catenin signaling pathway, presents itself as a potential target in treatment of cancer. In this study, a multi-stage *in silico* approach involving several steps was used to find potential TNKS1 inhibitors out of 6,000 DrugBank compounds. Following molecular docking, the top candidates were further filtered through binding interaction analysis with critical active-site residues and ADMET evaluation. Among 34 compounds, Ligand 16752640 is identified as the best candidate for having the most favorable pharmacokinetic and toxicity profile, showing the lowest predicted toxicity, minimal blood-brain barrier permeability, having the least plasma clearance, weak CYP inhibition, hERG inhibition and the best drug-likeness based on Lipinski's rule of five. Ligand 449087 and Tasosartan (60919) also showed promising characteristics. Overall, the identified lead compounds represent promising candidates for TNKS1-targeted therapy and provide a foundation for future experimental validation and potential drug repurposing in ovarian cancer treatment.

Key words: *Ovarian cancer, Tankyrase 1 (TNKS1), Virtual screening, Molecular docking, Drug repurposing, ADMET profiling, Wnt/β-catenin signaling, Lipinski's Rule*

Dedication

We dedicate this project to our families and well-wishers for their constant support, encouragement, and belief in us throughout this journey.

Acknowledgement

We express our deepest gratitude to Almighty Allah for His blessings, guidance, and strength throughout the completion of this project.

We would like to extend our sincere appreciation to our supervisor, Namara Mariam Chowdhury, Senior Lecturer, BRAC University, for her invaluable guidance, continuous support, and constructive feedback throughout this research project. Her expertise and encouragement have greatly contributed to the successful completion of this work.

We would also like to express our special thanks to Nashrah Mustafa, Senior Lecturer, BRAC University, for her constant assistance, insightful suggestions, and unwavering support from the beginning to the completion of this project. Her guidance played a significant role in helping us overcome challenges and remain motivated throughout the research process.

Finally, we are deeply grateful to our friends, Sazid, Nawshin, Mostakim and Utsha for their endless support, motivation, and belief in us throughout this journey. Their encouragement helped us remain focused and determined in achieving our goals. We sincerely appreciate everyone who contributed, directly or indirectly, to the successful completion of this project.

Table of Contents

List of Tables

List of Figures

List of Acronyms

ADMET	Absorption, Distribution, Metabolism, Excretion and Toxicity
ADT	AutoDockTools
AMES	Ames Mutagenicity Test
APC	Adenomatous Polyposis Coli
AXIN	Axis Inhibition Protein
BBB	Blood-Brain Barrier
CDK2	Cyclin-Dependent Kinase 2
CK1α	Casein Kinase 1 Alpha
CTNNB1	Catenin Beta 1 Gene
EOC	Epithelial Ovarian Carcinoma
H-HT	Human Hepatotoxicity
hERG	Human Ether-à-go-go-Related Gene
HIA	Human Intestinal Absorption
IUPAC	International Union of Pure and Applied Chemistry
nHA	Number of Hydrogen Bond Acceptors
nHD	Number of Hydrogen Bond Donors
PARP	Poly(ADP-ribose) Polymerase
PDB	Protein Data Bank

PPB	Plasma Protein Binding
SDF	Structure Data File
TNKS1	Tankyrase 1
TNKS2	Tankyrase 2
tPSA	Total Polar Surface Area

Chapter 1. Introduction

1.1 Prevalence of Ovarian Cancer

Ovarian cancer is one of the most fatal gynecologic cancers globally, with 324,603 cases diagnosed globally in 2022 (World Cancer Research Fund International, 2025). Although its global age-standardized incidence has decreased slightly over the last 30 years, incidence and mortality rates have continued to increase in certain low- and middle-income countries, and among women aged 20-39 years, the incidence rates and disability-adjusted life years have also risen steadily over the past 30 years (Li et al., 2026). Early symptoms are non-specific and the majority of cases are diagnosed at a late stage, which makes the case fatality ratio higher for the disease than warranted by its occurrence, thus emphasizing the need for new, mechanistically targeted treatment strategies.

1.2 Overview of Ovarian Cancer

Ovarian cancer occurs from the surface epithelium of the ovary or tissues like fallopian tube, peritoneum, most frequently from the surface epithelium (Al Qooz et al., 2024). Main treatment is based on cytoreductive surgery plus platinum-based chemotherapy, but as is the case with most cancers, chemoresistance and recurrence occurs in most patients (Lin et al., 2019) and is driving efforts to find new molecular drug targets.

1.3 Classification of Ovarian Cancer and Associated Signaling Pathways

Epithelial ovarian carcinoma (EOC) is the name given to this type of cancer which has five histotypes: high-grade serous, low-grade serous, mucinous, endometrioid, and clear cell carcinoma, with each type having different genetic drivers (Sciallis & Zhang, 2024). The dualistic model also classifies EOC into Type I (low-grade serous, mucinous, endometrioid, clear cell) which tend to be genetically stable and frequently harbor mutations in KRAS, PTEN, or CTNNB1, and Type II (most commonly high-grade serous) which are characterized by chromosomal instability and near-universal TP53 mutations (Kurman & Shih, 2016).

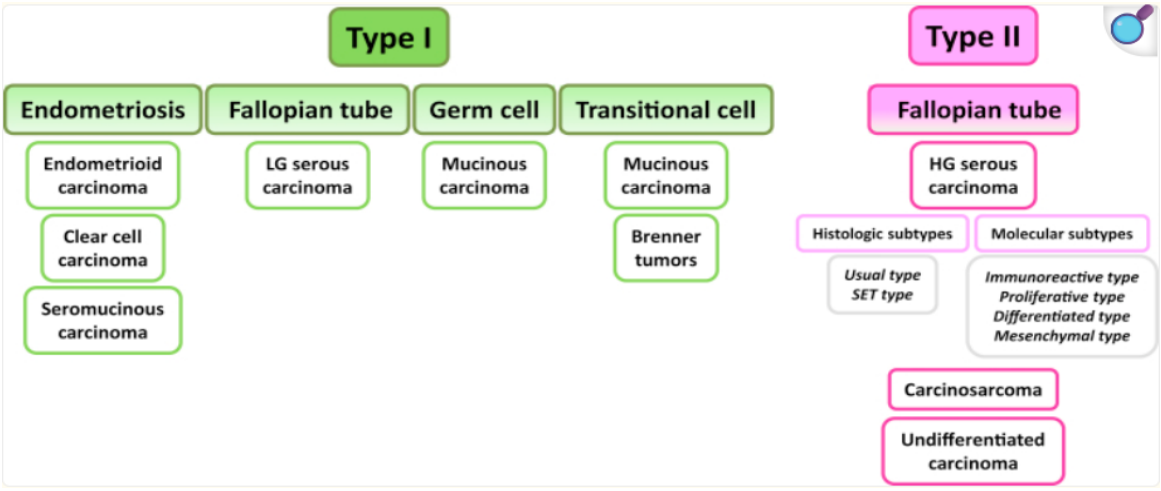

Figure 1: The revised dualistic model of ovarian carcinogenesis. (Kurman & Shih, 2016).

Among these subtype-specific changes, mutation of CTNNB1 which activates Wnt/β-catenin is the hallmark of endometrioid carcinoma, and its principal regulators, such as tankyrase, are also important in other ovarian cancer type histotypes, rendering them potential therapeutic targets in the context of ovarian cancer (Lin et al., 2019).

1.4 The Wnt/β-Catenin Pathway, Tankyrase, and Tankyrase 1

In the absence of Wnt ligands, β-catenin is bound to AXIN/APC/GSK3β/CK1α destruction complex and degraded; binding of Wnt ligands this complex is inhibited allowing β-catenin to accumulate and activate TCF/LEF target genes involved in proliferation (Riccio et al., 2016). The stability of AXIN is regulated by tankyrase 1 (TNKS1) and tankyrase 2 (TNKS2), PARP family enzymes that poly (ADP-ribosyl) ate AXIN and target it for degradation by RNF146, thus increasing Wnt output (Riccio et al., 2016; Bilbao-Aldaiturriaga et al., 2021).

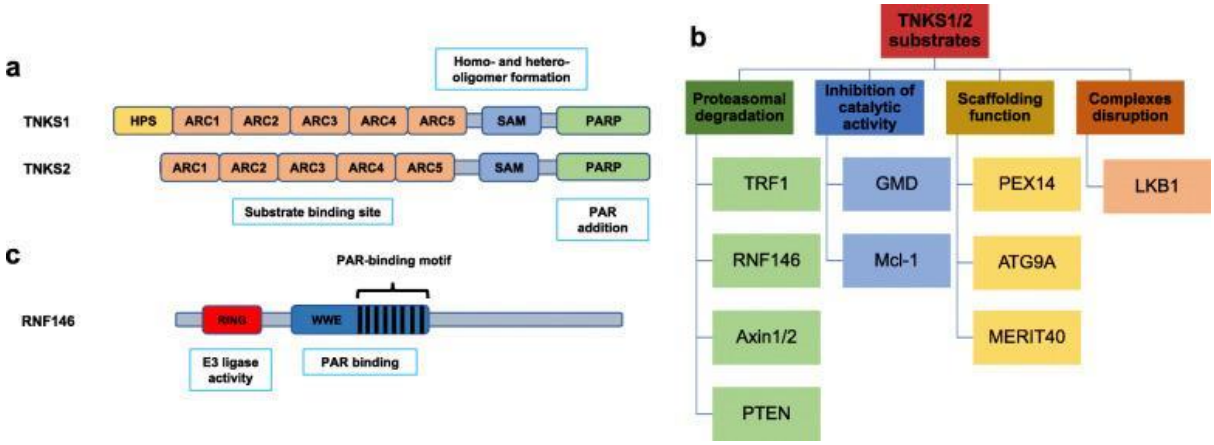

Figure 2: Tankyrase-mediated AXIN degradation in Wnt/β-catenin signaling. (Bilbao-Aldaiturriaga et al., 2021).

Tankyrase inhibition (such as done with XAV939) increases AXIN stability and inhibits the transcription of β-catenin (Huang et al., 2009). Tankyrase 1 is highly expressed in ovarian cancer tissues and associated with poor prognosis and its inhibition inhibits the proliferation, migration and invasion and enhances chemosensitivity (Lin et al., 2019).

1.5 Importance of Tankyrase 1 as a Target for Molecular Docking Studies

The PARP domain of TNKS1 is suitable for *in silico* docking because of the presence of a druggable pocket for binding the nicotinamide substrate, and several crystal structures with TNKS1 bound to inhibitors have been solved, facilitating the use of in silico docking for the virtual screening of compounds (Li et al., 2020). Because it controls AXIN stability, its inhibition suppresses Wnt output regardless of the upstream mutation, broadening its relevance across CTNNB1-driven and other Wnt-active ovarian tumors. Docking has already been tested on a large scale for tankyrase, with the compound LZZ-02 selected from a virtual screening of more than 13 million molecules and subsequently tested experimentally, proving it as a practical and effective means of finding inhibitors for this target (Li et al., 2020). Combined with its direct role in ovarian cancer cell growth, migration, and chemoresistance (Lin et al., 2019), these factors justify TNKS1 as the docking target of this study.

1.6 Research Gap

Most tankyrase-targeted drug discovery has focused on colorectal cancer and on TNKS2, leaving TNKS1-specific binding interactions and ADMET predictions in the context of ovarian cancer underexplored (Berishvili et al., 2020). Given high relapse rates after platinum-based therapy, this study addresses that gap through a structured in silico approach targeting TNKS1.

1.7 Aims and Objectives of the Study

This study aims to identify potential tankyrase 1 inhibitors against ovarian cancer through an in silico approach, with the following objectives:

1. To retrieve the tankyrase 1 catalytic domain structure and curate a ligand library for docking.
2. To perform molecular docking of the curated ligands against the tankyrase 1 active site and rank them by binding affinity against known inhibitors.
3. To evaluate the ADMET and drug-likeness profiles of top-ranked candidates and shortlist leads for future experimental validation in ovarian cancer.

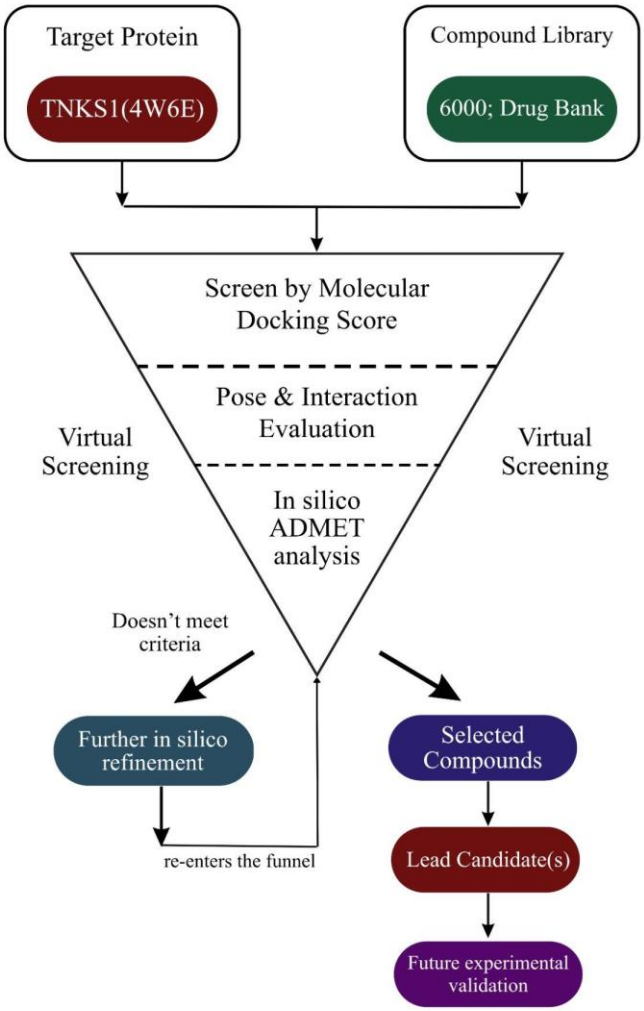

Figure 3: Overview of the research plan, illustrating the in silico virtual screening pipeline used to identify potential Tankyrase 1 (TNKS1) inhibitors against ovarian cancer.

Chapter 2. Methodology

2.1 Target Protein Selection and Retrieval

The three-dimensional crystal structure of Human Tankyrase 1 (TNKS1) bound with a small molecule inhibitor was retrieved from the RCSB Protein Data Bank (PDB) under the code **4W6E** (Berman H et al., 2000). This structure was chosen for its high resolution crystal and existence of a well-defined ligand-binding pocket within the PARP catalytic domain, providing a reliable template for further structure-based virtual screening.

The molecular target, TNKS1, was selected because it is a key molecule in the Wnt/β-catenin pathway that is often deregulated in ovarian cancer. TNKS1 induces the PARylation and degradation of AXIN (David S Wishart et al., 2018), a negative regulator of β-catenin, and thus maintains oncogenic signaling in an activated state. TNKS1 has been found to be overexpressed in ovarian cancer tissue, and inhibition of TNKS1 has been shown to inhibit tumor cell proliferation and promote apoptosis, placing it as an interesting and druggable anticancer target. Human Tankyrase 1 (PDB ID: 4W6E) was chosen as the target protein for the study. Tankyrase 1 (TNKS1), a member of the PARP superfamily, is essential for the Wnt/β-catenin pathway and is important in sustaining aberrant Wnt/β-catenin pathway activity that is observed in ovarian cancer. TNKS1 is a promising target for therapy due to its known over-expression in ovarian cancer tissues and its known role in tumor cell proliferation and survival. The structure of the 4W6E was selected because of the availability of high-resolution crystal data and the clearly defined druggable binding pocket which is occupied by a co-crystallized small molecule inhibitor, facilitating structure-based virtual screening.

2.2 Database and Software Utilized

Throughout this study, several databases and computational tools were used to retrieve the structural data, prepare molecular inputs, conduct docking simulations and assess the pharmacokinetic properties of potential compounds. The three dimensional structure of the target protein was downloaded from the RCSB Protein Data Bank (PDB) (https://www.rcsb.org/) and the library of ligands from DrugBank (https://www.drugbank.ca/). Protein preparation and visualization was performed in PyMOL (Schrödinger LLC, 2020) software. AutoDockTools (ADT) (Morris, G. M. et al., 2009) and Open Babel (O'Boyle, N. M. et al., 2011) were used for the preparation of the ligands and conversion of the file format. The

protein–ligand interactions were analyzed by Discovery Studio Visualizer and molecular docking was carried out using AutoDock Vina (Trott, O. & Olson, A. J., 2010). ADMETlab 3.0 (Fu et al., 2024) was used in silico ADMET profiling. A comprehensive list of all software and online tools used in this study is provided in Table 1.

SL	Software / Tool	Version	Purpose in This Study	Reference
1	RCSB Protein Data Bank (PDB)	-	Retrieval of target protein structure (4W6E)	Berman et al., 2000
2	DrugBank	v5.1	Source of 6,000 ligand compounds	Wishart et al., 2018
3	PubChem	-	Supplementary ligand structure retrieval	Kim et al., 2019
4	PyMOL	2.0	Protein visualization and preparation	Schrödinger LLC, 2020
5	AutoDockTools (ADT)	1.5.7	Ligand & receptor preparation; PDBQT conversion	Morris et al., 2009
6	Open Babel GUI	2.4.1	File format interconversion (SDF → PDBQT)	O'Boyle et al., 2011
7	AutoDock Vina, Perl	1.1.2	Molecular docking of 6,000 compounds against 4W6E	Trott & Olson, 2010
8	Discovery Studio Visualizer	21.1	Visualization of docking poses and protein–ligand interactions	BIOVIA, 2021
9	ADMETlab 3.0	3.0	In silico ADMET profiling of top-ranked hits	Fu et al., 2024

Table 1: Software and online tools used in the study

2.3 Protein Structure Preparation

The three-dimensional crystal structure of Human Tankyrase 1 was downloaded from the RCSB Protein Data Bank (PDB ID: 4W6E) in legacy PDB format. Protein preparation was performed using AutoDockTools (ADT) and PyMOL (Morris, G.M. et al., 2009). The structure was loaded and water molecules were removed prior to processing. Missing atoms were identified using the 'Check for Missing Atoms' function under the Edit > Miscellaneous menu. Polar hydrogen atoms were then added to the structure using the Add Polar Only option. Kollman charges were assigned as these charges are the standard charge set employed in AutoDock-based docking protocols for protein receptors and residue charges were verified and distributed using the Check Residue Charge function. Finally, the prepared receptor was exported in PDBQT format, saving the output as receptor.pdbqt for use in docking simulations. The PDBQT format encodes atomic coordinates alongside partial charges and atom types required for docking energy calculations.

Following these preparation steps, the receptor was considered ready for grid box configuration and molecular docking against the 6,000-compound DrugBank ligand library.

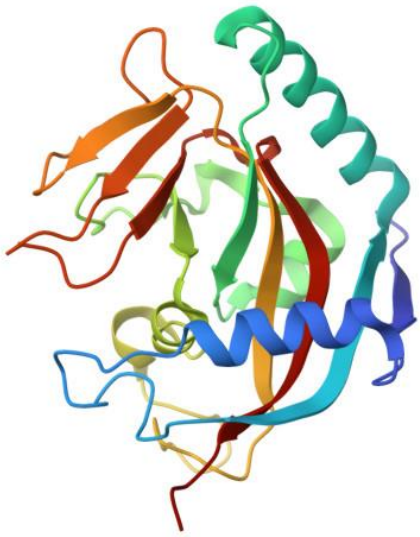

***Figure 4:** 4W6E_1, Represented by Chain A*

2.4 Ligand Dataset Preparation

A database containing about 6,000 compounds in SDF format was downloaded from DrugBank (https://go.drugbank.com/). The database included drugs from different pharmacological classes, such as Proton Pump Inhibitors, Antidepressants, Antiparkinson Drugs, Bronchodilators, Antidotes, Anti-thyroid Drugs, Natural Compounds, Local Anesthetics, Anti-neoplastic Agents, Statins, Diuretics, Antidiabetic Drugs, Nonsteroidal Anti-inflammatory Drugs, Antihypertensive Drugs, Anti-fungal Drugs, Antihistamines, Analgesics, Anti-viral Drugs, Anti-mycobacterial Drugs, Anti-emetics, Anti-convulsants, Antibiotics, and Alpha Blockers. SDF files were then converted into PDBQT format, which is needed as input for AutoDock Vina and Perl, using Open Babel GUI (v2.4.1).

2.5 Molecular Docking Simulation

The binding affinity of the 6,000-compound ligand library with the Human Tankyrase 1 crystal structure (PDB ID: 4W6E) was evaluated by molecular docking. A **Perl script** that is called iteratively for each ligand PDBQT file in the folder of prepared ligands, with the receptor file, grid box parameters, and docking configurations as arguments and automatically merges all the docking results into one output file containing the binding affinities for each ligand. With this automation, it ensured consistency across all docking runs and significantly cut processing time. Binding affinities were reported in kilocalories per mole (kcal/mol). The more negative affinities, the greater the binding interaction between the ligand and receptor.

The batch docking script was executed via the Windows Command Prompt using the following command sequence:

```
cd /
C:\>cd "Thesis"
C:\Thesis>perl vina_windows_pl.txt
Ligand_file: Ligand.txt
```

Here, the working directory was first changed to the root drive **(cd/)**, followed by navigation into the project folder named "Thesis" **(cd "Thesis")**, where the receptor file, ligand library, and Perl script were stored. The batch docking script **(vina_windows_pl.txt)** was then executed using the command perl vina_windows_pl.txt. The script subsequently prompted for the ligand file name, at which point Ligand.txt, a text file containing the list of all 6,000 prepared ligand PDBQT files was supplied as input. The script then iteratively called

AutoDock Vina for each listed ligand against the prepared receptor **(receptor.pdbqt)** using the predefined grid box parameters, and compiled the resulting binding affinity values into a single consolidated output file.

To validate the docking protocol and set a reference binding affinity, docking was initially done on the co-crystallized reference inhibitor of 4W6E prior to screening the full library. The binding affinity score of the reference inhibitor was taken as the cutoff, compounds which have docking scores equal to or less (more negative) than the reference were shortlisted for further analysis. This was a reference based cutoff that guarantees that the hits selected had binding affinities comparable to or greater than a known active inhibitor of the target protein.

The docking grid box was chosen such that the centre of it was in the active site of 4W6E and the X, Y, Z Cartesian coordinates were reported in literature for the binding site of Tankyrase 1 (Bijani S, et al., 2022). The complete grid box and docking parameters used in AutoDock Vina are summarized in Table 2.

Parameter	Value	Unit
Center X (center_x)	15.54	Å
Center Y (center_y)	20.84	Å
Center Z (center_z)	-27.09	Å
Size X (size_x)	25	Å
Size Y (size_y)	25	Å
Size Z (size_z)	25	Å
Number of Binding Modes (num_modes): 10		
Energy Range (energy_range): 4kcal/mol		

Table 2. Grid box and docking parameters used for screening against 4W6E (Bijani et al., 2022)

2.6 Protein-Ligand Interaction Analysis

Protein-ligand interactions of compounds demonstrating favorable docking scores were analyzed using **Discovery Studio Visualizer** to evaluate the nature and quality of their binding within the active site of **4W6E**. Key non-covalent interactions, including hydrogen bonds, hydrophobic contacts, π-stacking, and electrostatic interactions, were examined for each docked ligand. Interacting amino acid residues were documented and compared against those formed by the reference inhibitors **3J5** and **AZ6102**, with particular attention paid to shared residues and analogous bonding patterns. Compounds sharing a greater number of common interacting residues with the reference inhibitors were considered more promising candidates, while those exhibiting unfavorable steric clashes (bumps) within the binding pocket - indicative of poor structural fit or strained, energetically unfavorable contacts between the ligand and receptor atoms were excluded from further consideration, regardless of their docking score. This exclusion criterion ensured that only compounds with both favorable binding energies and structurally sound, sterically compatible binding poses were advanced to the subsequent ADMET evaluation stage.

2.7 Pharmacokinetic Profiles

Favorable binding affinity and protein-ligand interaction profiles alone are insufficient to qualify a compound as a viable drug candidate; a molecule must also possess acceptable pharmacokinetic behavior and a tolerable toxicity profile to have realistic therapeutic potential (Kennedy, T., 1997). Accordingly, the pharmacokinetic features and toxicity characteristics of the compounds shortlisted from the docking and interaction analysis stages were systematically evaluated using ADMETlab 3.0 (https://admetlab3.scbdd.com/), a comprehensive web-based platform for the in silico prediction of Absorption, Distribution, Metabolism, Excretion, and Toxicity properties.

Chapter 3. Results

3.1 Overview of the Virtual Screening Workflow

This chapter presents the outcomes of the multi-stage in silico screening pipeline employed to identify potential Tankyrase 1 (TNKS1) inhibitors from the DrugBank compound library. Out of the 6,000 compounds initially docked against the 4W6E receptor, sequential filtering based on binding affinity, protein-ligand interaction profiling, and pharmacokinetic/toxicity evaluation progressively narrowed the candidate pool to a final set of promising lead compounds. The overall screening funnel is summarized below.

Stage 1: Molecular Docking

6,000 DrugBank compounds docked against 4W6E using AutoDock Vina

↓

Cutoff applied: binding affinity < -13.5 kcal/mol (reference inhibitor score)

↓

100 compounds shortlisted

Stage 2: Visual Inspection

100 compounds visualized using BIOVIA Discovery Studio

↓

Poses evaluated for binding orientation and validity

↓

60 compounds retained

Stage 3: Protein-Ligand Interaction Analysis

60 compounds compared against reference inhibitors 3J5 and AZ6102

↓

Common amino acid residue interactions identified

↓

34 compounds with highest interactions selected

Stage 4: ADMET Profiling

34 compounds evaluated using ADMETlab 3.0

↓

Lipinski's Rule of Five, absorption, distribution, and toxicity assessed

↓

Final lead candidates identified

With each step of this pipeline, the criteria for filtering the compounds became increasingly stringent - initially being energetic (affinity to binding site), then structural (quality of interaction and number of residues involved) and lastly pharmacokinetics (drug-likeness). All results from each step of this pipeline are described in the next sections.

3.2 Analysis of Docking Results: Reference Inhibitor Score

Following the molecular docking of all 6,000 DrugBank compounds against the Human Tankyrase 1 receptor (PDB ID: 4W6E), the co-crystallized reference inhibitor 3J5 and AZ6102 were independently docked against the same receptor to establish a benchmark binding affinity for hit selection. AZ6102 and 3J5 were used as reference ligands because they are established tankyrase inhibitors and provide benchmark docking scores for evaluating screened compounds (Johannes et al., 2015). The docking scores of 3J5 and AZ6102 were -13.8 and -13.2 kcal/mol, respectively, and were used as reference values. The top 100 compounds with the most favorable (most negative) binding affinity scores from the full docking run were shortlisted for further analysis (Table 3).

Sl. No.	Ligand ID	Affinity Value (kcal/mol)
1.	15991573_ligand	-14.5
2.	10389239_ligand	-13.7
3.	9823454_ligand	-13.5
4.	128919_ligand	-13.4
5.	24875320_ligand	-13.3
6.	21081761_ligand	-13.2
7.	6918314_ligand	-13
8.	447767_ligand	-12.9
9.	11485656_ligand	-12.8
10.	16750097_ligand	-12.8

11.	657077_ligand	-12.8
12.	11567682_ligand	-12.7
13.	2384_ligand	-12.7
14.	10172943_ligand	-12.6
15.	17758361_ligand	-12.6
16.	23658582_ligand	-12.6
17.	25023705_ligand	-12.6
18.	445480_ligand	-12.6
19.	45268539_ligand	-12.6
20.	16122633_ligand	-12.5
21.	24882195_ligand	-12.5
22.	25134257_ligand	-12.5
23.	10156987_ligand	-12.4
24.	11633167_ligand	-12.4
25.	449087_ligand	-12.4
26.	11291932_ligand	-12.3
27.	11507920_ligand	-12.3
28.	16752640_ligand	-12.3
29.	24941253_ligand	-12.3
30.	4566_ligand	-12.3
31.	5326924_ligand	-12.3
32.	9998128_ligand	-12.3
33.	11840906_ligand	-12.2
34.	447656_ligand	-12.2
35.	447734_ligand	-12.2
36.	10477723_ligand	-12.1
37.	15942655_ligand	-12.1
38.	24812717_ligand	-12.1
39.	24832041_ligand	-12.1
40.	445849_ligand	-12.1
41.	11544170_ligand	-12
42.	11560856_ligand	-12

43.	11992146_ligand	-12
44.	15602701_ligand	-12
45.	24764434_ligand	-12
46.	24864821_ligand	-12
47.	5287979_ligand	-12
48.	695906_ligand	-12
49.	10062702_ligand	-11.9
50.	16040279_ligand	-11.9
51.	6105620_ligand	-13.2
52.	448889_ligand	-13
53.	446605_ligand	-12.9
54.	17753851_ligand	-12.8
55.	2280_ligand	-12.8
56.	2281_ligand	-12.8
57.	657141_ligand	-12.8
58.	447476_ligand	-12.7
59.	6398417_ligand	-12.7
60.	446399_ligand	-12.5
61.	445843_ligand	-12.3
62.	10050566_ligand	-12.2
63.	444746_ligand	-12.2
64.	447524_ligand	-12.2
65.	65999_ligand	-12.2
66.	2605_ligand	-12
67.	445756_ligand	-12
68.	447488_ligand	-12
69.	448327_ligand	-12
70.	5591_ligand	-12
71.	1282_ligand	-11.9
72.	150311_ligand	-11.9
73.	156419_ligand	-11.8
74.	68723_ligand	-11.8

75.	6957673_ligand	-11.8
76.	9887303_ligand	-11.8
77.	4369359_ligand	-11.7
78.	447478_ligand	-11.7
79.	5287994_ligand	-11.7
80.	5496989_ligand	-11.7
81.	5510_ligand	-11.7
82.	57030_ligand	-11.7
83.	2267_ligand	-11.6
84.	445459_ligand	-11.6
85.	446752_ligand	-11.6
86.	5496599_ligand	-11.6
87.	60919_ligand	-11.6
88.	6918296_ligand	-11.6
89.	4034_ligand	-11.5
90.	4369285_ligand	-11.5
91.	444031_ligand	-11.5
92.	444698_ligand	-11.5
93.	446201_ligand	-11.5
94.	446276_ligand	-11.5
95.	446978_ligand	-11.5
96.	447731_ligand	-11.5
97.	448605_ligand	-11.5
98.	124087_ligand	-11.4
99.	1543_ligand	-11.4
100.	445986_ligand	-11.4

Table 3. Maximum 100 values after doing molecular docking of 6000 drugs

3.3 Protein-Ligand Interaction Results

3.3.1 Visual Inspection of Docking Poses

The 100 top ranked compounds that made it to the molecular docking stage were then visually inspected and studied for protein-ligand interactions using **BIOVIA Discovery Studio Visualizer** software. The 2D interaction diagram generated by Discovery Studio was analyzed for each compound to assess the quality, type and biological relevance of the predicted binding pose in the 4W6E active site.

The 2D interaction diagrams clearly and comprehensively showed all non-covalent interactions between each ligand and the rest of the surrounding active site residues, such as hydrogen bond, hydrophobic contact, π-stacking interaction, and electrostatic forces. Most importantly, these diagrams also highlighted any unfavorable steric contacts, those contacts involving atoms of the ligand that are placed in energetically uncomfortable, geometrically incompatible positions with the receptor atoms which are known as "bumps" are excluded. Following this inspection, 60 compounds were selected that showed structurally sound, sterically compatible binding poses with meaningful interaction profiles within the Tankyrase 1 active site. These 60 compounds were compared for interaction analysis against the reference inhibitors 3J5 and AZ6102 in the next step.

3.3.2 Interaction Comparison with References and Identification of common residues

To further refine the candidate pool, the protein-ligand interaction profiles of the 60 visually validated compounds were compared against those of the two reference inhibitors, 3J5 and AZ6102, both of which are established Tankyrase 1 inhibitors with co-crystallized well-characterized binding modes within the 4W6E active site.

Ligand	Name	Distance	Category	Type
AZ6102	:UNL1:H3 - A:SER1221:OG	3.04897	Hydrogen Bond	Carbon Hydrogen Bond
	:UNL1:H4 - A:GLY1185:O	2.72616	Hydrogen Bond	Carbon Hydrogen Bond
	:UNL1:H5 - A:SER1221:OG	2.49803	Hydrogen Bond	Carbon Hydrogen Bond
	:UNL1:H6 - A:TYR1213:O	2.93827	Hydrogen Bond	Carbon Hydrogen Bond
	:UNL1:H6 - A:SER1221:OG	2.88033	Hydrogen Bond	Carbon Hydrogen Bond
	A:TYR1213 - :UNL1	5.18243	Hydrophobic	Pi-Pi Stacked
	A:TYR1224 - :UNL1	3.58401	Hydrophobic	Pi-Pi Stacked
	:UNL1 - A:TYR1224	4.10297	Hydrophobic	Pi-Pi Stacked
	A:HIS1184 - :UNL1:C	4.14454	Hydrophobic	Pi-Alkyl
	A:TYR1224 - :UNL1:C	5.32821	Hydrophobic	Pi-Alkyl
	:UNL1 - A:ALA1215	5.09991	Hydrophobic	Pi-Alkyl
	:UNL1 - A:LYS1220	5.31977	Hydrophobic	Pi-Alkyl
3J5	A:HIS1184:HD1 - :UNL1:O	3.04171	Hydrogen Bond	Conventional Hydrogen Bond
	A:GLY1185:HN - :UNL1:O	1.96213	Hydrogen Bond	Conventional Hydrogen Bond
	:UNL1:H - A:GLY1185:O	2.10361	Hydrogen Bond	Conventional Hydrogen Bond
	A:HIS1184 - :UNL1	5.03246	Hydrophobic	Pi-Pi Stacked
	A:TYR1213 - :UNL1	5.62641	Hydrophobic	Pi-Pi Stacked
	A:TYR1224 - :UNL1	3.81463	Hydrophobic	Pi-Pi Stacked
	A:TYR1224 - :UNL1	4.49483	Hydrophobic	Pi-Pi Stacked
	:UNL1 - A:ALA1215	4.99406	Hydrophobic	Pi-Alkyl
	:UNL1 - A:LYS1220	5.12566	Hydrophobic	Pi-Alkyl

Table 4: Protein-ligand interaction profile of the reference inhibitors (3J5 and AZ6102) with Human Tankyrase 1 (4W6E).

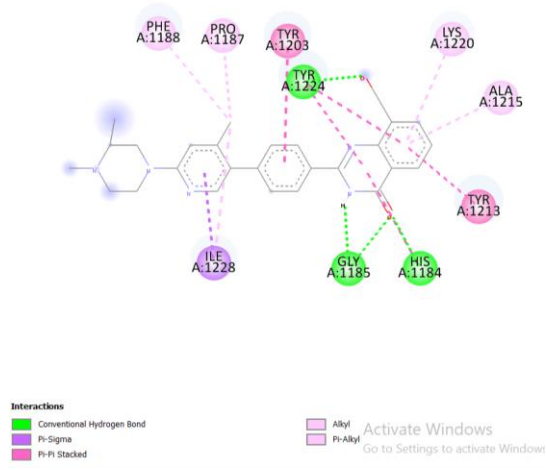

Figure 5: 2D structure of 3J5 (2-[4-[6-[(3S)-3,4-dimethylpiperazin-1-yl]-4-methyl-3-pyridinyl]phenyl]-8-(hydroxymethyl)-3H-quinazolin-4-one)

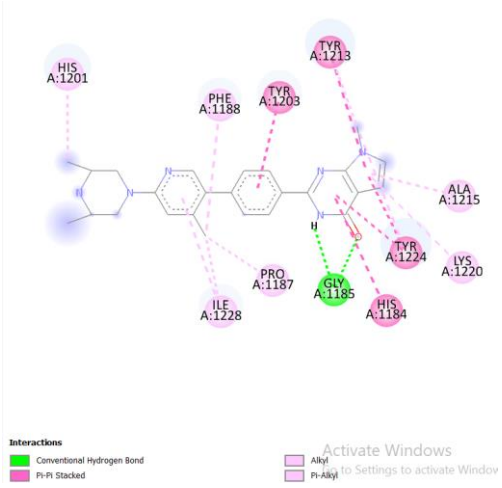

Figure 6: 2D structure of AZ6102 (2-[4-[6-[(3R,5S)-3,5-dimethylpiperazin-1-yl]-4-methyl-3-pyridinyl]phenyl]-7-methyl-3H-pyrrolo[2,3-d]pyrimidin-4-one)

The 2D interaction diagrams of 3J5 and AZ6102 were first explored separately individually, in Discovery Studio Visualizer to determine which amino acid residues interact with each reference inhibitor. A set of seven amino acid residues was found in both of these interaction profiles, which included **Ser1221, Gly1185, Tyr1213, Tyr1224, His1184, Ala1215, and Lys1220** (Table 4). Both 3J5 and AZ6102 are validated co-crystallised TNKS1 inhibitors, so these common intermolecular interactions were taken as the standard set of interacting residues required for productive TNKS1 inhibition and used for screening the 60 candidate compounds. The 60 candidate compounds were then evaluated against this reference residue set in a two-step screening process:

1. **Presence screening**: Each of the 60 compounds was first matched to determine whether it formed an interaction with at least one of the seven common reference residues (Ser1221, Gly1185, Tyr1213, Tyr1224, His1184, Ala1215, Lys1220). Compounds that are showing no overlap with this residue set were excluded from further consideration.
2. **Frequency ranking:** Among the compounds that showed overlap, the number of common reference residues engaged by each compound was counted. Compounds interacting with a greater number of these seven residues were considered to more closely replicate the binding behavior of the validated reference inhibitors, and were therefore ranked as stronger candidates.

Applying this two-step residue-matching criterion to the 60 candidate compounds yielded a final shortlist of 34 compounds that exhibited the highest degree of common amino acid residue interaction with the reference inhibitors 3J5 and AZ6102 and were subsequently carried forward for in silico ADMET profiling.

3.3.3 Two-Dimensional Structures of the Finalized 34 Compounds

The 2D chemical structures of the 34 compounds finally shortlisted on the basis of binding affinity and common amino acid residue interactions with the reference inhibitors (3J5 and AZ6102) are presented in **figure 7 to figure 40**. These structures are provided to give a clear visual reference of the chemical scaffolds carried forward for in silico ADMET profiling, as discussed in Section 3.4.

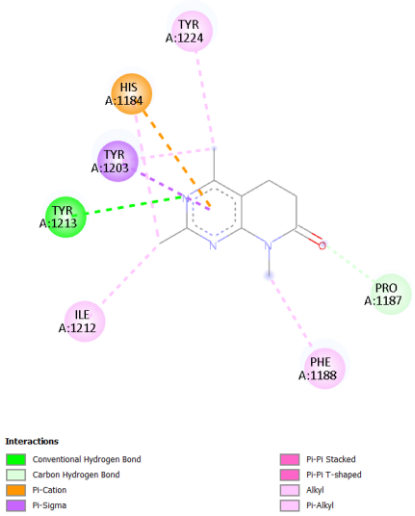

Figure 7: 2D structure of Tasosartan

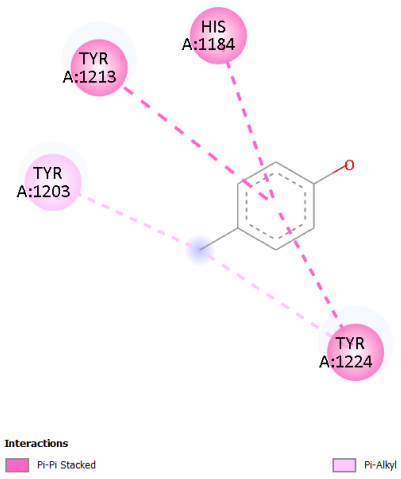

Figure 8: 2D structure of Bentiromide

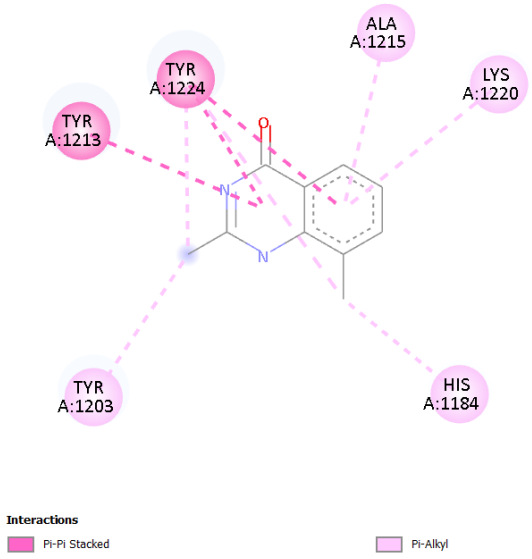

Figure 9: 2D structure of N-(1,3-benzothiazol-2-yl)-1-ethyl-3-methylpyrazole-4-sulfonamide

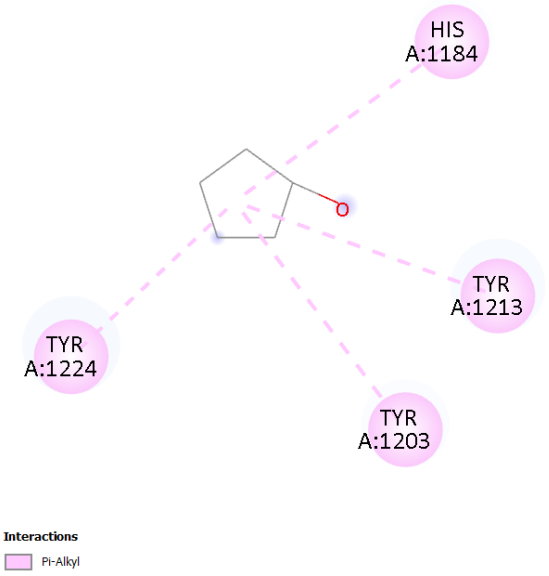

Figure 10: 2D structure of 6-chloro-2-(3-cyclopentyloxy-2-hydroxyphenyl)-1H-indole-5-carboximidamide

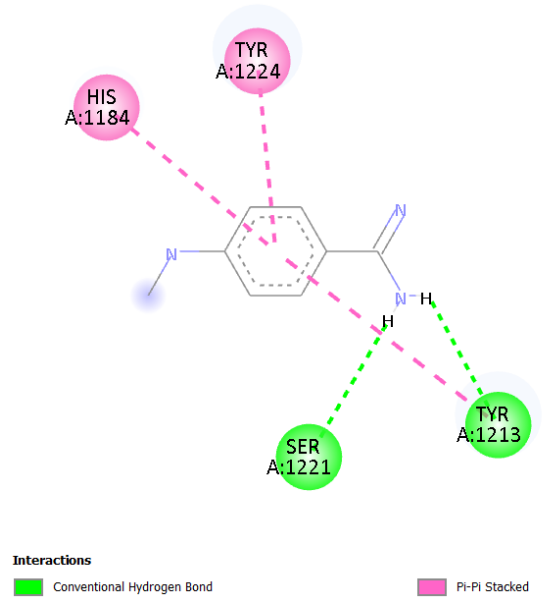

Figure 11: 2D structure of 4-[[1-methyl-5-[(2-methylbenzimidazol-1-yl)methyl]benzimidazol-2-yl]methylamino]benzenecarboximidamide

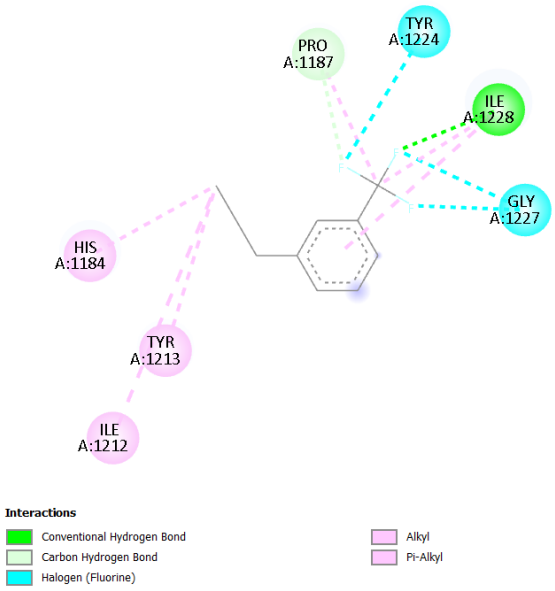

Figure 12: 2D structure of Cinacalcet

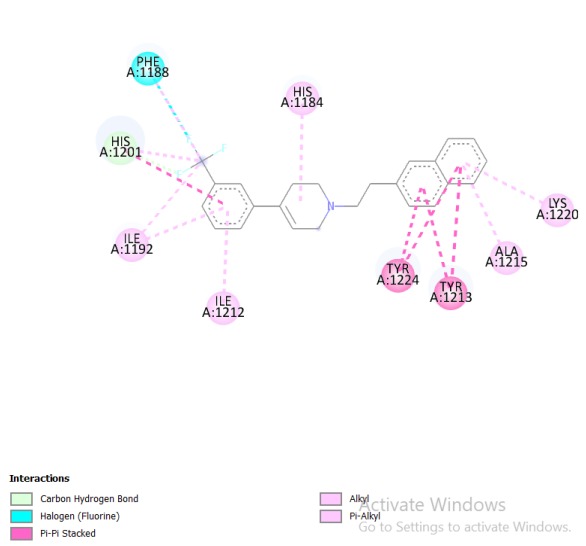

Figure 13: 2D structure of Xaliproden

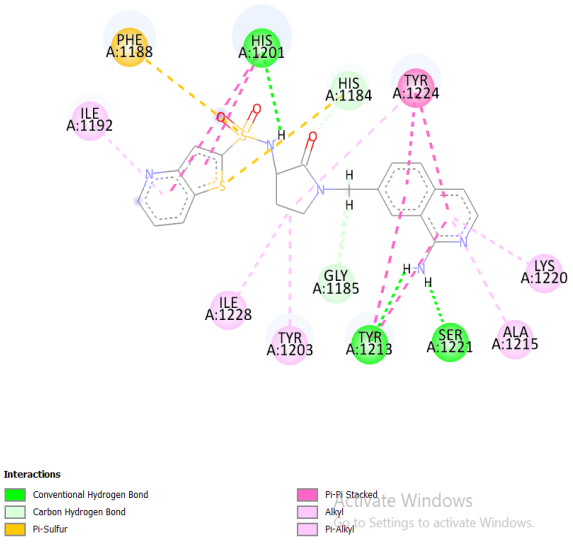

Figure 14: 2D structure of N-[(3S)-1-[(1-aminoisoquinolin-7-yl)methyl]-2-oxopyrrolidin-3-yl]thieno[3,2-b]pyridine-2-sulfonamide

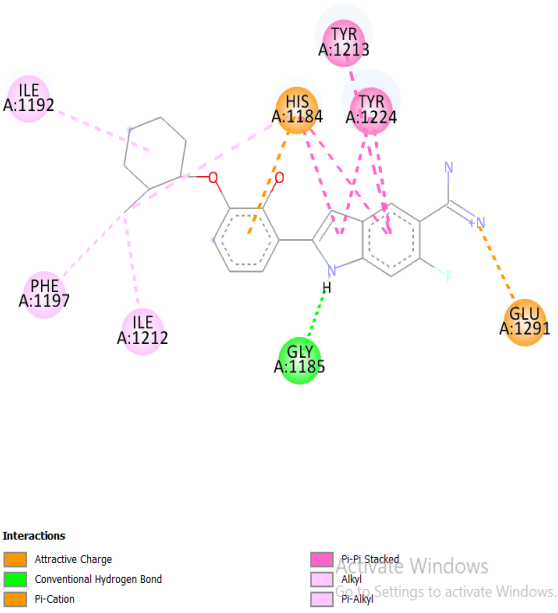

Figure 15: 2D structure of 6-fluoro-2-[2-hydroxy-3-[(1S,2S)-2-methylcyclohexyl]oxyphenyl]-1H-indole-5-carboximidamide

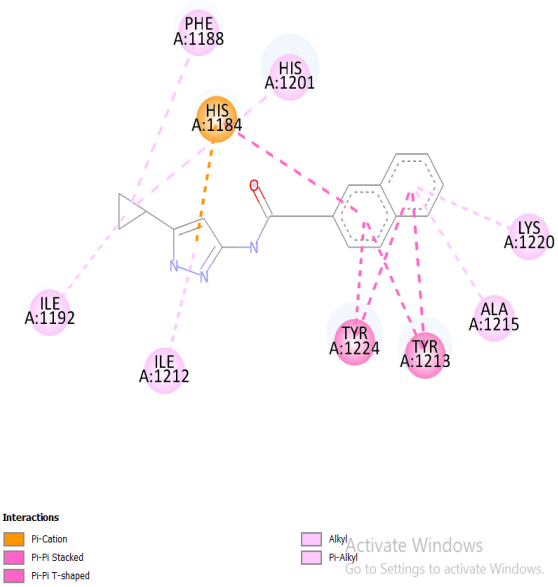

Figure 16: 2D structure of N-(5-cyclopropyl-1H-pyrazol-3-yl)-2-naphthalen-2-ylacetamide

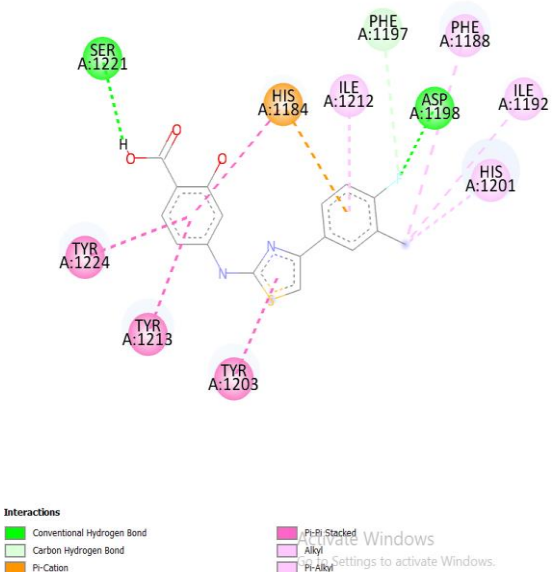

Figure 17: 2D structure of 4-[[4-(4-fluoro-3-methylphenyl)-1,3-thiazol-2-yl]amino]-2-hydroxybenzoic acid

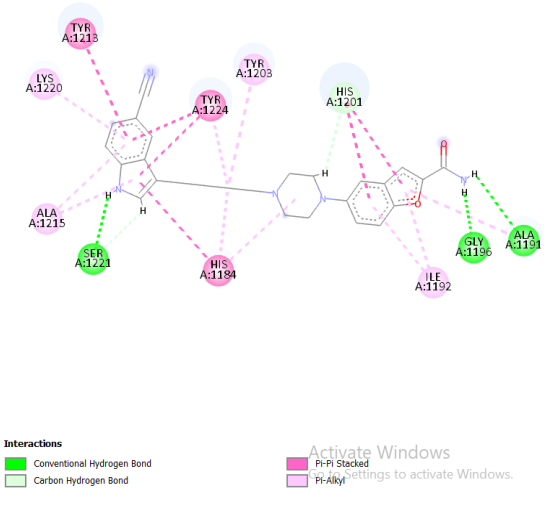

Figure 18: 2D structure of Vilazodone

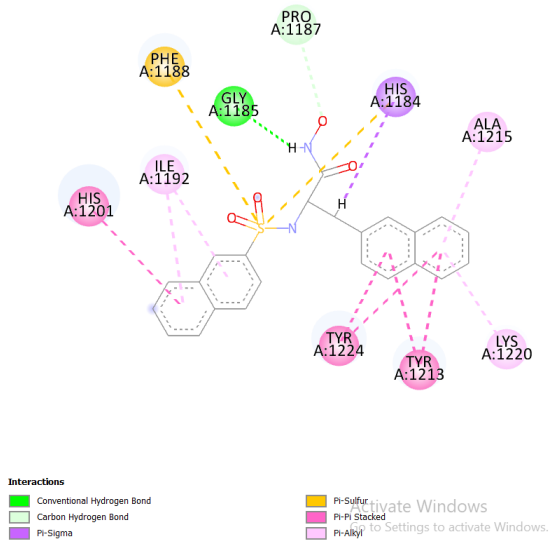

Figure 19: 2D structure of (2R)-N-hydroxy-3-naphthalen-2-yl-2-(naphthalen-2-ylsulfonylamino)propanamide

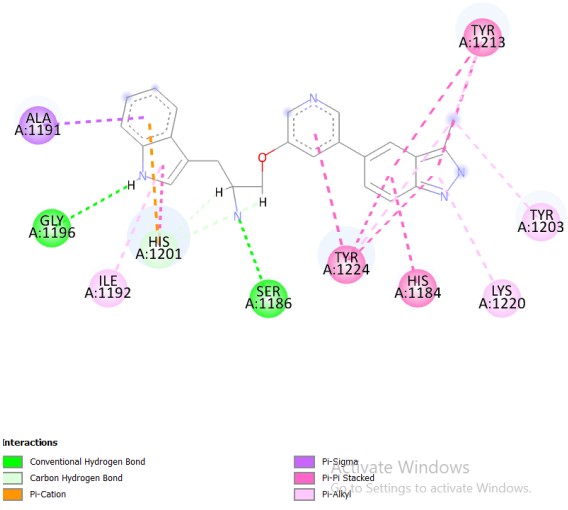

Figure 20: 2D structure of (2S)-1-(1H-indol-3-yl)-3-[[5-(3-methyl-2H-indazol-5-yl)-3-pyridinyl]oxy]propan-2-amine

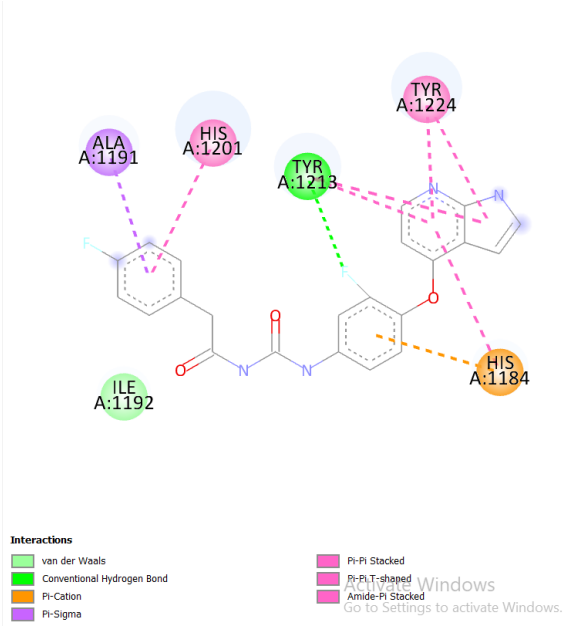

Figure 21: 2D structure of 2-(4-fluorophenyl)-N-[[3-fluoro-4-(1H-pyrrolo[2,3-b]pyridin-4-yloxy)phenyl]carbamoyl]acetamide

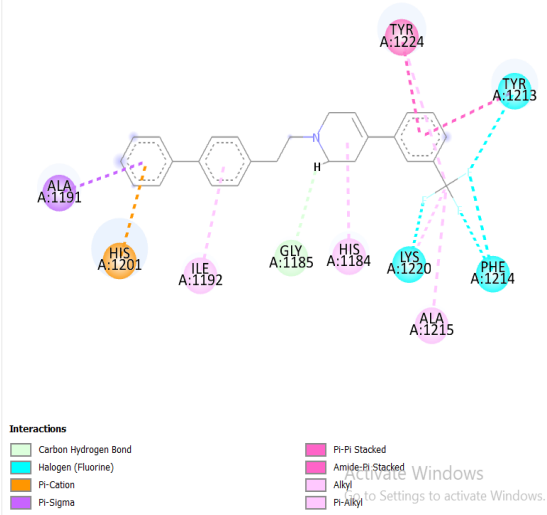

Figure 22: 2D structure of Paliroden

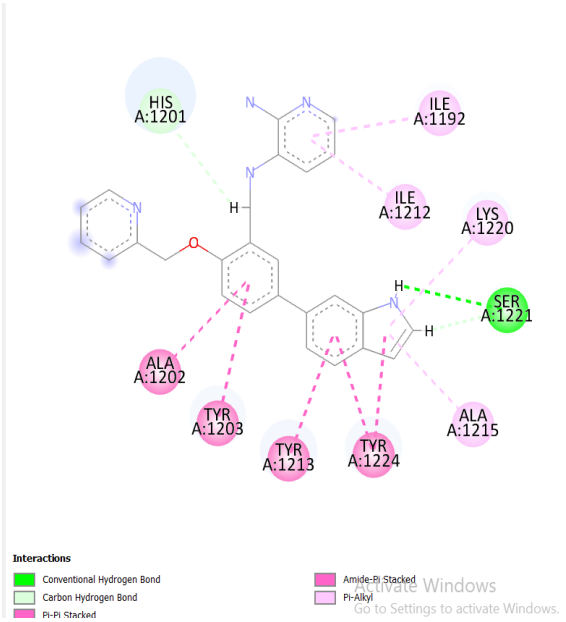

Figure 23: 2D structure of 3-N-[[5-(1H-indol-6-yl)-2-(pyridin-2-ylmethoxy)phenyl]methyl]pyridine-2,3-diamine

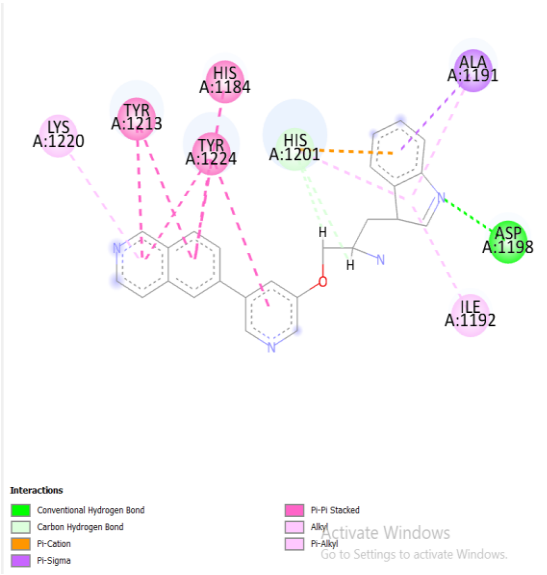

Figure 24: 2D structure of (2S)-1-(3H-indol-3-yl)-3-[(5-isoquinolin-6-yl-3-pyridinyl)oxy]propan-2-amine

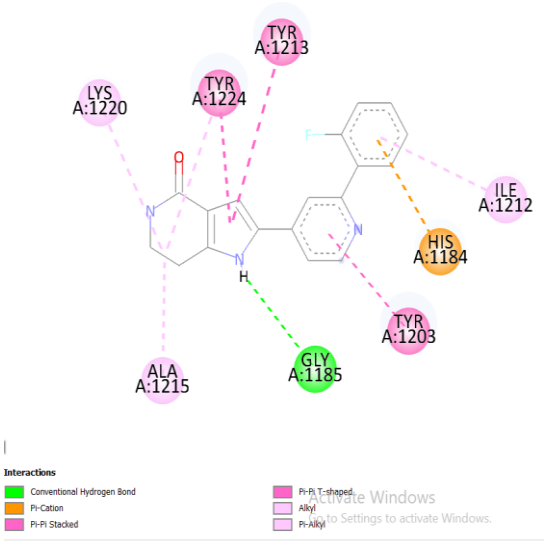

Figure 25: 2D structure of 2-[2-(2-fluorophenyl)-4-pyridinyl]-1,5,6,7-tetrahydropyrrolo[3,2-c]pyridin-4-one

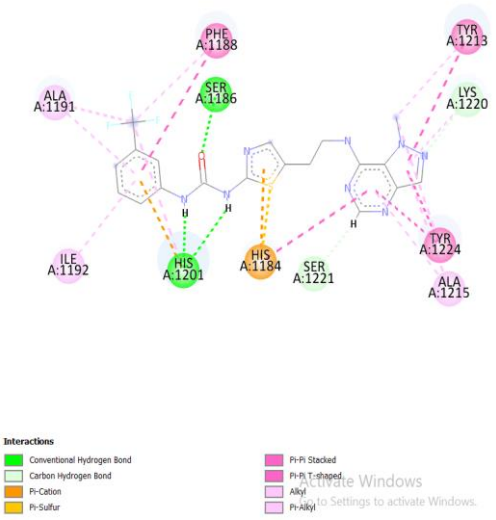

Figure 26: 2D structure of 1-[5-[2-[(1-methylpyrazolo[4,5-d]pyrimidin-7-yl)amino]ethyl]-1,3-thiazol-2-yl]-3-[3-(trifluoromethyl)phenyl]urea

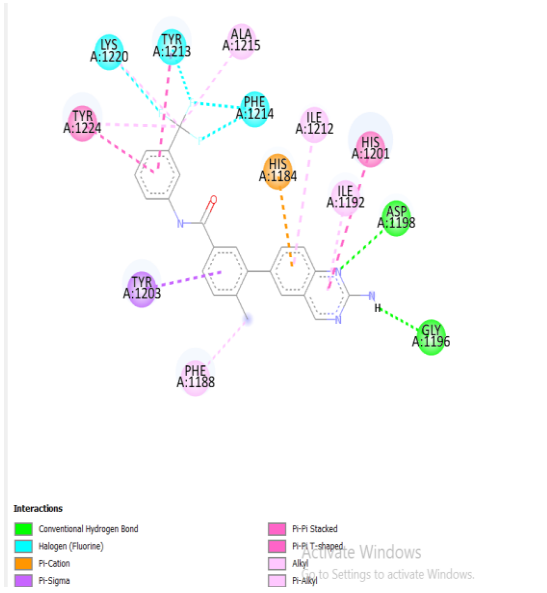

Figure 27: 2D structure of 3-(2-aminoquinazolin-6-yl)-4-methyl -N-[3-(trifluoromethyl)phenyl]benzamide

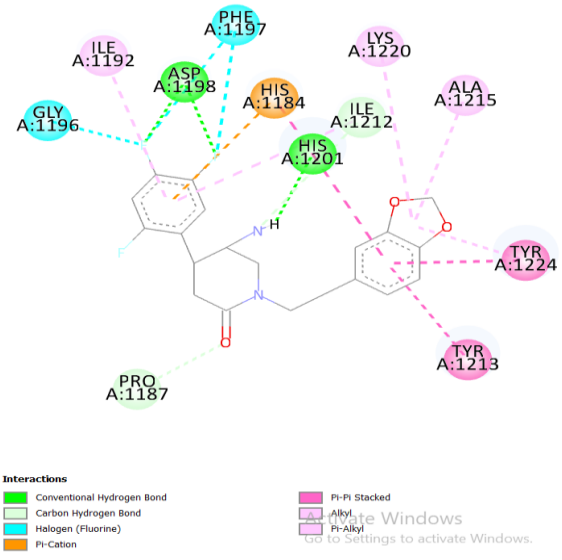

Figure 28: 2D structure of (4R,5R)-5-amino-1-[2-(1,3-benzodioxol-5-yl)ethyl]-4-(2,4,5-trifluorophenyl)piperidin-2-one

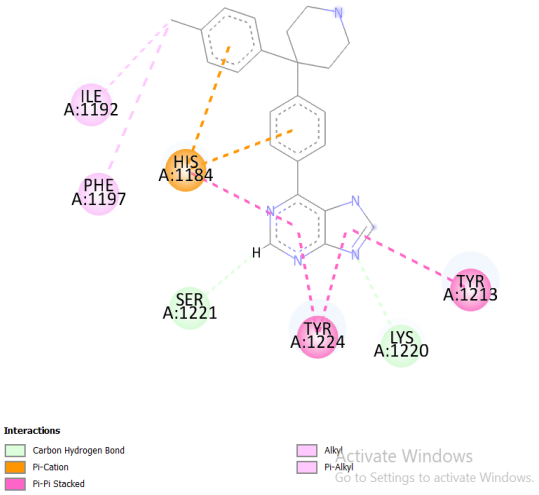

Figure 29: 2D structure of 6-[4-[4-(4-chlorophenyl)piperidin-4 -yl]phenyl]-7H-purine

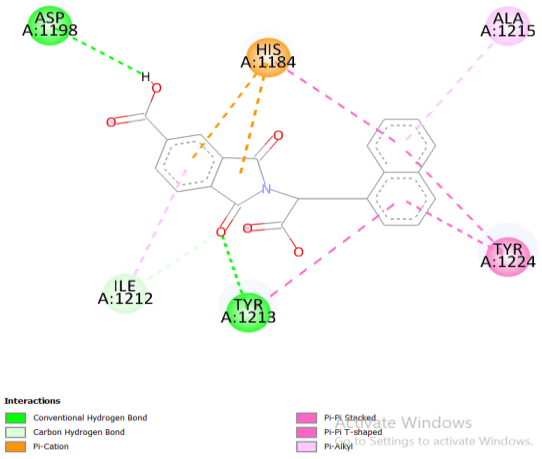

Figure 30: 2D structure of 2-[(1R)-1-carboxy-2-naphthalen-1-ylethyl] -1,3-dioxoisoindole-5-carboxylic acid

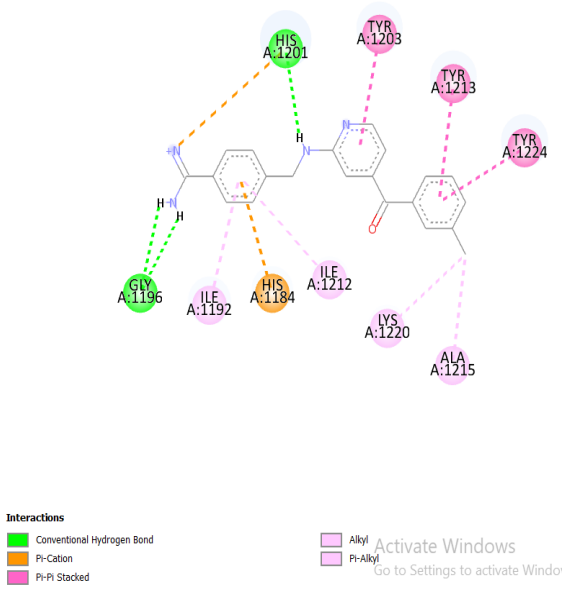

Figure 31: 2D structure of 4-[[[4-(3-methylbenzoyl)-2-pyridinyl] amino]methyl]benzenecarboximidamide

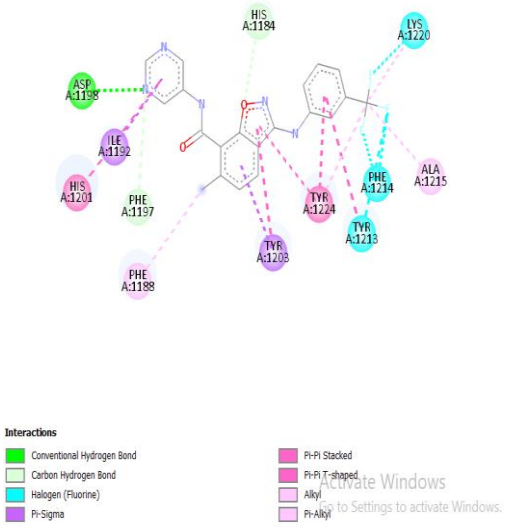

Figure 32: 2D structure of 6-chloro-N-pyrimidin-5-3-[3-(trifluoromethyl)anilino]-1,2-benzoxazole-7 -carboxamide

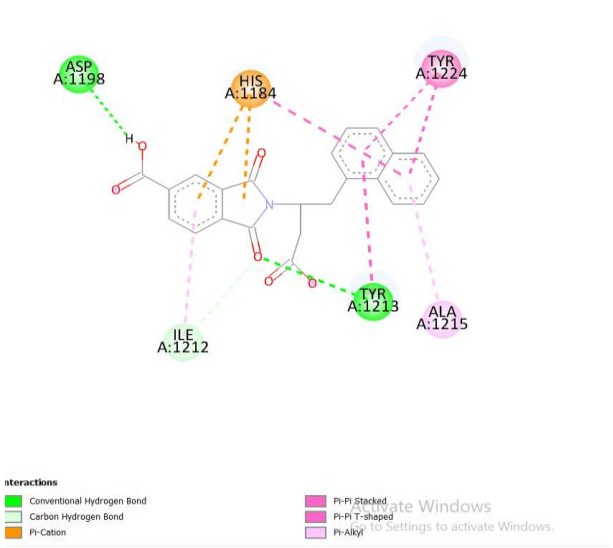

Figure 33: 2D structure of 2-[(2R)-1-carboxy-3-naphthalen-1-ylpropan-2-yl]-1,3-dioxoisoindole-5-carboxylic acid

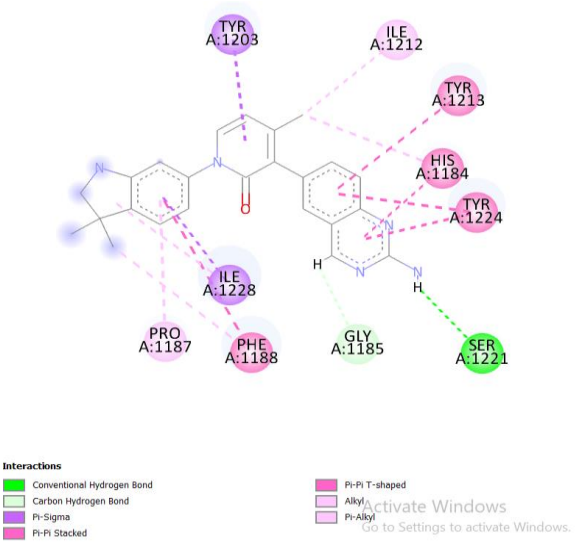

Figure 34: 2D structure of 3-(2-aminoquinazolin-6-yl)(3,3-dimethyl-1,2-dihydroindol-6-yl)-4-methylpyridin-2-one

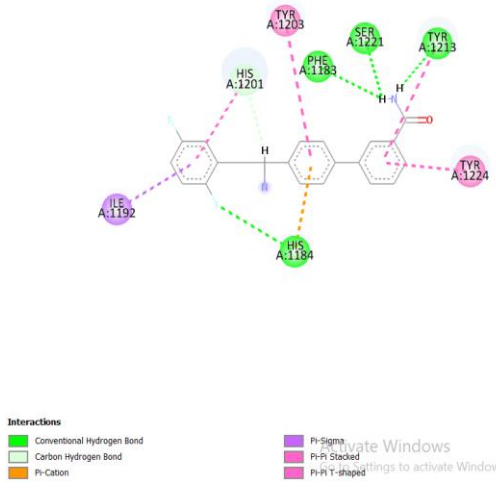

Figure 35: 2D structure of 3-[4-[(1R)-1-amino-2-(2,5-difluorophenyl)ethyl]phenyl]benzamide

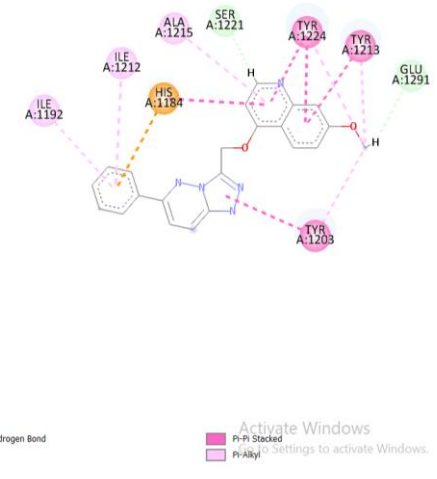

Figure 36: 2D structure of 7-methoxy-4-[(6-phenyl-[1,2,4]triazolo[4,3-b]pyridazin-3-yl)methoxy]quinoline

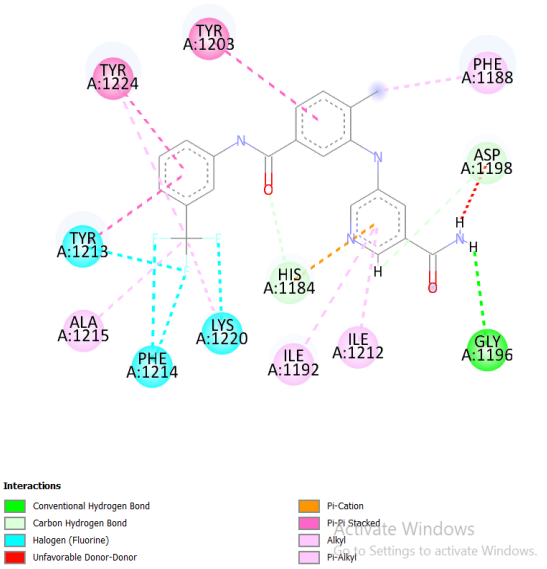

Figure 37: 2D structure of 5-[2-methyl-5-[[3-(trifluoromethyl)phenyl] carbamoyl]anilino]pyridine-3-carboxamide

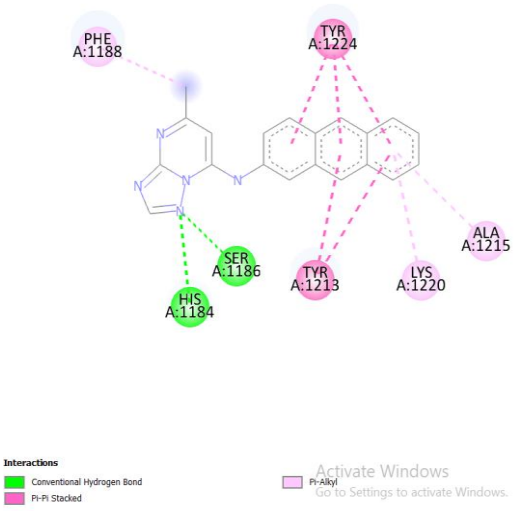

Figure 38: 2D structure of N-anthracen-2-yl-5-methyl-[1,2,4]triazolo[1,5-a]pyrimidin-7-amine

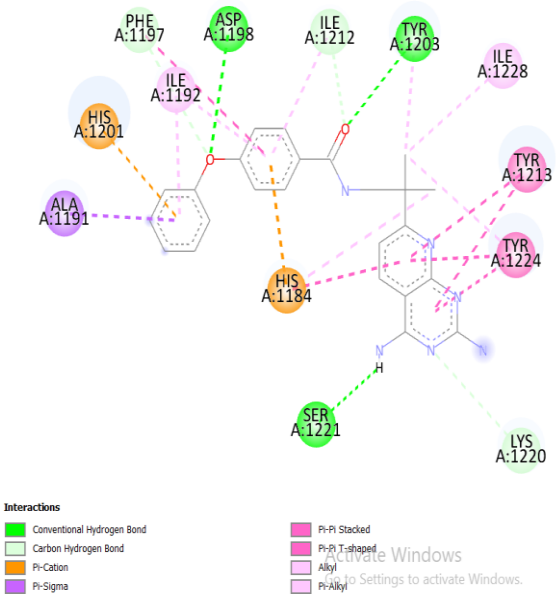

Figure 39: 2D structure of N-[2-(2,4-diaminopyrido[2,3-d]pyrimidin-7-yl)-2-methylpropyl]-4-phenoxybenzamide

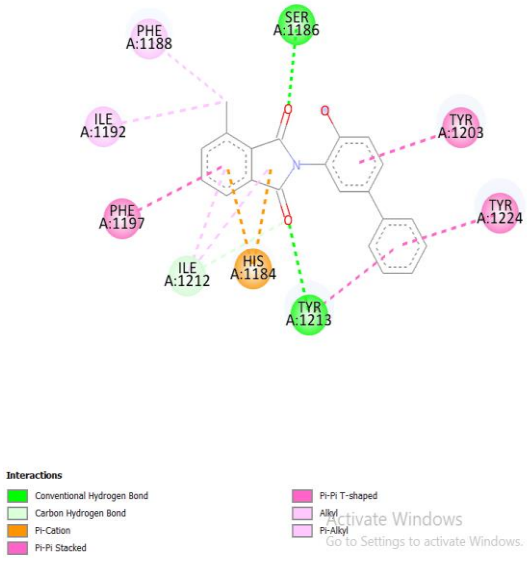

Figure 40: 2D structure of 2-(2-hydroxy-5-phenylphenyl)-4-methylisoindole-1,3-dione

3.4 Pharmacokinetic and Toxicity (ADMET) Results

A crucial stage in the development of new drugs is the early resolution of pharmacokinetic and toxicological characteristics of medication candidates. In order to achieve this goal, all 34 of the chosen drugs were evaluated for their pharmacokinetic (ADME) parameters and drug toxicity predictions using ADMET lab 3.0 (Fu et al., 2024), as indicated in table 7.

IUPAC/ Generic Name	Ligand	Absorption		Distribution		Metabolism			Elimination		Toxicity		
		caco2	HIA	PPB	BBB	CYP2C9-inh	CYP3A4-inh	CYP3A4-sub	Cl-plasma	t0.5	AMES	H-HT	hERG
Tasosartan	**60919**	-4.703	0.000002	95.327	0.929	0.019	0.004	1.000	3.238	0.764	0.687	0.805	0.349
Xaliproden	**128919**	-4.879	0.0003	98.224	0.995	0.161	0.297	0.557	11.423	2.032	0.277	0.843	0.980
Cinacalcet	**156419**	-5.264	0.000005	96.121	0.003	0.00001	0.058	0.994	7.161	0.276	0.156	0.980	0.874
N-[(3S)-1-[(1-aminoisoquinolin-7-yl)methyl]-2-oxopyrrolidin-3-yl]thieno[3,2-b]pyridine-2-sulfonamide	**445480**	-5.591	0.005	90.304	0.002	0.045	0.896	0.998	4.464	0.869	0.920	0.865	0.499
4-[[1-methyl-5-[(2-methylbenzimidazol-1-yl)methyl]benzimidazol-2-yl]methylamino]benzenecarboximidamide	**445756**	-6.014	0.002	83.550	0.106	0.00002	0.004	0.702	3.655	0.659	0.473	0.968	0.930

6-fluoro-2-[2-hydroxy-3-[(1S,2S)-2-methylcyclohexyl]oxyphenyl]-1H-indole-5-carboximidamide	**445849**	-5.944	0.004	75.358	0.001	0.000002	0.0001	0.000001	5.488	0.475	0.251	0.864	0.552
6-chloro-2-(3-cyclopentyloxy-2-hydroxyphenyl)-1H-indole-5-carboximidamide	**447488**	-5.838	0.002	94.726	0.114	0.000002	0.001	0.0000003	5.062	0.569	0.110	0.673	0.746
N-(5-cyclopropyl-1H-pyrazol-3-yl)-2-naphthalen-2-ylacetamide	**449087**	-4.830	0.001	98.731	0.182	0.575	0.192	0.651	5.780	0.703	0.575	0.755	0.334
4-[[4-(4-fluoro-3-methylphenyl)-1,3-thiazol-2-yl]amino]-2-hydroxybenzoic acid	**695906**	-5.098	0.006	99.909	0.004	0.920	0.315	0.006	2.010	0.990	0.570	0.772	0.212
N-(1,3-benzothiazol-2-yl)-1-ethyl-3-methylpyrazole-4-sulfonamide	**4469359**	-5.313	0.003	98.465	0.282	1.000	1.000	0.876	3.506	0.599	0.541	0.849	0.082

Vilazodone	**6918314**	-5.200	0.0004	95.101	0.891	0.000001	0.00001	1.000	5.207	0.890	0.722	0.976	0.997
Bentiromide	**6957673**	-5.949	0.001	95.316	0.00001	0.010	0.0002	0.001	1.719	1.112	0.345	0.895	0.254
(2R)-N-hydroxy-3-naphthalen-2-yl-2-(naphthalen-2-ylsulfonylamino)propanamide	**9823454**	-5.957	0.00002	97.457	0.00001	0.973	0.999	0.445	6.456	1.040	0.973	0.963	0.307
(2S)-1-(1H-indol-3-yl)-3-[[5-(3-methyl-2H-indazol-5-yl)-3-pyridinyl]oxy]propan-2-amine	**10172943**	-5.409	0.000	56.331	0.016	0.0005	0.997	0.006	6.122	0.461	0.668	0.958	0.544
2-(4-fluorophenyl)-N-[[3-fluoro-4-(1H-pyrrolo[2,3-b]pyridin-4-yloxy)phenyl]carbamoyl]acetamide	**11560856**	-5.375	0.005	98.916	0.116	1.000	0.194	0.044	1.026	1.107	0.607	0.858	0.278
Paliroden	**11567682**	-4.919	0.001	98.398	0.964	0.218	0.037	0.547	11.094	1.654	0.242	0.861	0.991

3-N-[[5-(1H-indol-6-yl)-2-(pyridin-2-ylmethoxy)phenyl]methyl]pyridine-2,3-diamine	**11633167**	-5.354	0.003	97.046	0.232	0.00004	0.828	0.001	6.763	0.557	0.829	0.885	0.773
(2S)-1-(3H-indol-3-yl)-3-[(5-isoquinolin-6-yl-3-pyridinyl)oxy]propan-2-amine	**11840906**	-5.121	8×10^{-7}	71.231	0.136	0.035	1.000	0.0002	5.706	0.611	0.822	0.972	0.915
2-[2-(2-fluorophenyl)-4-pyridinyl]-1,5,6,7-tetrahydropyrrolo[3,2-c]pyridin-4-one	**11992146**	-5.022	0.002	98.044	0.127	0.318	0.000	0.002	4.606	0.892	0.926	0.803	0.451
1-[5-[2-[(1-methylpyrazolo[4,5-d]pyrimidin-7-yl)amino]ethyl]-1,3-thiazol-2-yl]-3-[3-(trifluoromethyl)phenyl]urea	**15602701**	-4.947	0.005	98.161	0.848	0.383	0.867	0.035	3.444	0.907	0.225	0.946	0.577
3-(2-aminoquinazolin-6-yl)-4-methyl-N-[3-	**15991573**	-4.657	0.00005	98.143	0.226	0.047	0.011	0.779	5.946	0.785	0.596	0.917	0.827

(trifluoromethyl)phenyl]benzamide													
(4R,5R)-5-amino-1-[2-(1,3-benzodioxol-5-yl)ethyl]-4-(2,4,5-trifluorophenyl)piperidin-2-one	**16040279**	-5.351	4×10^{-7}	88.653	0.966	0.002	0.996	0.517	3.867	0.764	0.758	0.965	0.730
6-[4-[4-(4-chlorophenyl)piperidin-4-yl]phenyl]-7H-purine	**16122633**	-4.906	0.00001	89.770	0.956	1×10^{-8}	0.000	0.997	7.267	0.752	0.285	0.914	0.895
2-[(1R)-1-carboxy-2-naphthalen-1-ylethyl]-1,3-dioxoisoindole-5-carboxylic acid	**16752640**	-5.031	0.001	98.209	0.0002	0.0002	0.00001	0.0002	0.693	1.349	0.210	0.932	0.043
4-[[[4-(3-methylbenzoyl)-2-pyridinyl]amino]methyl]benzenecarboximidamide	**17758361**	-5.526	0.003	90.021	0.085	0.001	0.086	0.0003	5.306	0.815	0.156	0.855	0.919

6-chloro-N-pyrimidin-5-yl-3-[3-(trifluoromethyl)anilino]-1,2-benzoxazole-7-carboxamide	**23658582**	-5.088	0.0004	98.359	0.371	0.929	0.774	0.017	0.930	1.807	0.163	0.964	0.859
2-[(2R)-1-carboxy-3-naphthalen-1-ylpropan-2-yl]-1,3-dioxoisoindole-5-carboxylic acid	**24764434**	-5.104	0.041	98.076	0.00002	0.041	0.000003	0.0002	1.668	1.166	0.576	0.883	0.058
3-(2-aminoquinazolin-6-yl)-1-(3,3-dimethyl-1,2-dihydroindol-6-yl)-4-methylpyridin-2-one	**24812717**	-4.680	0.0002	94.380	0.091	0.0005	0.003	0.999	6.244	0.438	0.938	0.893	0.706
3-[4-[(1R)-1-amino-2-(2,5-difluorophenyl)ethyl]phenyl]benzamide	**24832041**	-5.201	0.000	91.616	0.173	0.0001	0.0002	0.003	5.788	0.819	0.744	0.979	0.859
7-methoxy-4-[(6-phenyl-[1,2,4]triazolo[4,3-b]pyridazin-3-yl)methoxy]quinoline	**24864821**	-4.695	0.0002	98.621	0.935	0.988	0.214	0.293	3.983	0.786	0.831	0.687	0.723

5-[2-methyl-5-[[3-(trifluoromethyl)phenyl]carbamoyl]anilino]pyridine-3-carboxamide	**24875320**	-5.218	0.00001	97.318	0.102	1.000	0.613	0.00001	3.429	1.106	0.234	0.901	0.919
N-anthracen-2-yl-5-methyl-[1,2,4]triazolo[1,5-a]pyrimidin-7-amine	**24882195**	-4.705	0.0001	92.510	0.178	0.054	0.748	0.377	4.547	0.625	0.837	0.828	0.490
N-[2-(2,4-diaminopyrido[2,3-d]pyrimidin-7-yl)-2-methylpropyl]-4-phenoxybenzamide	**25023705**	-5.183	0.00004	92.567	0.157	0.907	0.00002	0.145	5.234	0.602	0.847	0.930	0.888
2-(2-hydroxy-5-phenylphenyl)-4-methylisoindole-1,3-dione	**25134257**	-4.545	0.046	98.472	0.009	0.984	0.396	0.003	4.738	0.872	0.716	0.666	0.169

Table 5: Pharmacokinetic features (In silico ADMET) predictions.

Absorption was first assessed through Caco-2 permeability, which predicts intestinal uptake, with better absorption through the intestinal epithelium is indicated by higher permeability (few negative values) (Di & Kerns, 2010). The majority of compounds had values between -4.5 and -6.0 log cm/s, indicating moderate to good intestinal permeability. Compounds with values below −5.8 may show decreased oral absorption, while Tasosartan (Ligand 60919) (−4.70) and N-(5-cyclopropyl-1H-pyrazol-3-yl)-2-naphthalen-2-ylacetamide (Ligand 449087) (−4.83) showed more favorable permeability. Human Intestinal Absorption (HIA), in which higher values indicate better intestinal uptake. HIA indicates the likelihood of absorption after oral administration. While some of the screened compounds showed poor HIA probabilities, 2-[(2R)-1-carboxy-3-naphthalen-1-ylpropan-2-yl]-1,3-dioxoisoindole-5-carboxylic acid (Ligand 24764434) (0.041) and 2-(2-hydroxy-5-phenylphenyl)-4-methylisoindole-1,3-dione (Ligand 25134257) (0.046) showed relatively higher predicted intestinal absorption.

With respect to distribution, the fraction of drug bound to plasma proteins is shown by Plasma Protein Binding (PPB) (Artursson & Karlsson, 1991). Most compounds showed PPB values above 90%, suggesting strong protein binding. High PPB can decrease the percentage of free, pharmacologically active medication while also prolonging systemic circulation. The majority of candidates had PPB ratings between 90 and 99%. On the other hand, compounds' capacity to reach the central nervous system is predicted by Blood-Brain Barrier (BBB) penetration (Di et al., 2003). High BBB penetration probabilities were shown by compounds including Tasosartan (0.929), Vilazodone (0.891), Paliroden (0.964), and Xaliproden (0.995), indicating possible CNS activity. However, compounds like Bentiromide (0.000014) and Ligand 16752640 (0.00017) showed minimal BBB penetration, which can be advantageous for non-CNS therapeutic targets like the one this study examined. Since Tankyrase 1 inhibition for ovarian cancer therapy is a peripherally acting mechanism, compounds predicted to be non-BBB permeant were considered pharmacologically favorable, as CNS exposure offers no therapeutic benefit and may introduce unnecessary neurological risk (Summerfield et al., 2014).

Metabolic stability was assessed through predicted inhibition of cytochrome P450 enzymes CYP2C9 and CYP3A4, since inhibition of these isoforms may result in clinically relevant drug-drug interactions (Zanger & Schwab, 2013; Guengerich, 2008), where lower inhibition probabilities being preferred. A number of several compounds showed little capacity to inhibit CYP2C9, such as Cinacalcet (8.32×10^{-1}) and Ligand 445849 (1.70×10^{-1}), whereas compounds

like Ligand 24875320 (0.9998) and Ligand 4469359 (0.9999) showed a significant likelihood of CYP2C9 inhibition. A similar pattern was observed for CYP3A4 inhibition, where several compounds demonstrated negligible inhibitory activity, whereas Ligands 4469359, 9823454, 11840906, and 16040279 showed high CYP3A4 inhibitory potential. Since about half of commercially available medications are metabolized by CYP3A4; lower inhibition probabilities suggest a decreased risk of interactions. In addition, CYP3A4 Substrate Probability was examined, since compounds that are predicted to be CYP3A4 substrates may be extensively metabolized by the liver. Vilazodone (0.9999), Cinacalcet (0.9938), and Tasosartan (0.9999) all showed high substrate probability, indicating metabolism via CYP3A4-mediated pathways. Although substrate status does not necessarily indicate poor pharmacokinetic behavior, it may predispose compounds to CYP3A4-mediated drug-drug interactions.

Excretion-related parameters, namely plasma clearance and half-life, were used to characterise the rate and duration of systemic drug elimination (Di & Kerns, 2009; Obach et al., 2008). Lower clearance levels typically signify extended systemic exposure. While Xaliproden (11.42) and Paliroden (11.09) demonstrated rapid predicted clearance, ligand 16752640 had the lowest clearance (0.693), indicating a possibly prolonged duration of action. Correspondingly, predicted half-Life (t½) values that indicate the duration of systemic exposure and greater half-lives typically justify less frequent dosing. The majority of compounds had half-lives that were between 0.4 and 2.0 hours. The half-lives of Xaliproden (2.03) and Paliroden (1.65) were much longer.

Toxicity assessment encompassed mutagenicity, hepatotoxicity, and cardiotoxicity endpoints. Mutagenic potential is predicted using the Ames test (Mortelmans & Zeiger, 2000), with lower values referring to a lower risk of mutagenicity. Ames toxicity probability were comparatively low for Ligand 447488 (0.110), Cinacalcet (0.156), Ligand 17758361 (0.156), and Ligand 23658582 (0.163). Human Hepatotoxicity (H-HT), by which the probability of liver toxicity is estimated by hepatotoxicity prediction (Chen et al., 2013; Vinken, 2015), where lower values are being preferred. Compared to the majority of other candidates, Ligand 25134257 (0.666), Ligand 447488 (0.673), and Tasosartan (0.805) showed relatively lower hepatotoxicity probability. Finally hERG inhibition, a critical cardiotoxicity marker because inhibition of the hERG potassium channel may lead to QT interval prolongation and fatal arrhythmias (Sanguinetti & Tristani-Firouzi, 2006; Redfern et al., 2003); for which lower values are

preferred. QT interval refers to the duration between ventricular depolarization and repolarization on an electrocardiogram (Raschi et al., 2009). The ligands with the lowest hERG inhibition probability were 16752640 (0.043), 24764434 (0.058), 4469359 (0.082), and 695906 (0.212). Vilazodone (0.997), Paliroden (0.991), Xaliproden (0.980), and a number of other compounds, on the other hand, showed a significant predicted risk of hERG inhibition.

With poor BBB penetration, minimal CYP inhibition, low Ames mutagenicity, very low hERG inhibition, and low plasma clearance, **Ligand 16752640** showed the most favorable overall ADMET profile among the evaluated drugs. Additionally, **Ligand 449087** and **Tasosartan (60919)** showed acceptable pharmacokinetic characteristics. However, while having favorable permeability properties, compounds like Vilazodone, Paliroden, and Xaliproden demonstrated substantial hERG inhibition probability, which may limit their usefulness as lead candidates. These results imply that Ligand **16752640** deserves additional study using experimental validation and molecular dynamics simulations.

3.5 Lipinski's Rule of Five: Drug-Likeness Analysis

The molecular weight (MW), lipophilicity (LogP), number of hydrogen bond acceptors (nHA), number of hydrogen bond donors (nHD), and total polar surface area (tPSA) of the 34 shortlisted candidate compounds are shown in Table 8 and compared with the Lipinski's Rule of Five (Lipinski et al., 1997).

Parameter-by-Parameter Analysis

1. **Molecular Weight (MW ≤ 500 g/mol)**: All 34 compounds satisfied this criterion, with values ranging from 291.14 (Ligand 449087) to 462.12 (Ligand 15602701). None of the compounds in the candidate set approached or exceeded the 500 g/mol cut-off, which means the entire candidate set is in the suitable zone of membrane permeability.
2. **Lipophilicity (LogP ≤ 5):** The vast majority of the compounds had LogP values much lower than the threshold. Two compounds (Ligand 128919, LogP = 5.40 and Ligand 11567682, LogP = 5.77) were found to be beyond the LogP ≤ 5 limit, thus being the only compound with Lipinski violation out of the whole set.
3. **Hydrogen Bond Acceptors (nHA ≤ 10):** No compounds failed this criterion, and the range of the hydrogen bond acceptors (nHA) was from 4 to 9. The highest number (9) was with Ligand 15602701, which is acceptable.

4. **Hydrogen Bond Donors (nHD ≤ 5):** All compounds complied with this parameter as well, with nHD values ranging from 0 to 5. No compound exceeded the threshold.

Additionally, tPSA is frequently cited alongside Lipinski's original rule as a predictor of oral absorption, although not being a part of it. Compounds with a tPSA value at or below 140 Å² are typically linked with good oral bioavailability (Veber et al., 2002). All 34 compounds were below this cutoff, and their positive absorption potential was further supported by tPSA values ranging from 3.24 to 129.04 Å². All 34 compounds (100%) fit the usual interpretation of Lipinski's Rule of Five, which states that a molecule is deemed drug-like if it violates no more than one of the four characteristics (Lipinski et al., 1997).

Ligand	MW	logP	nHA	nHD	tPSA
60919	411.18	1.97973115	8	1	100.55
128919	381.17	5.40184744	1	0	3.24
156419	357.17	4.996708006	1	1	12.03
445480	453.09	1.109264273	8	3	118.28
445756	423.22	1.750993281	7	4	97.54
445849	381.19	2.913492347	5	5	95.12
447488	369.12	3.193228685	5	5	95.12
449087	291.14	3.197751585	4	2	57.78
695906	344.06	4.868143427	5	3	82.45
4469359	322.06	2.119484902	6	1	76.88
6918314	441.22	3.012577076	7	3	102.29
6957673	404.14	2.254689793	7	4	115.73
9823454	420.11	3.092326291	6	3	95.5
10172943	397.19	2.919680647	6	4	92.61
11560856	422.12	4.125591108	7	3	96.11
11567682	407.19	5.76674445	1	0	3.24
11633167	421.19	3.91754599	6	4	88.85
11840906	394.18	2.705032956	5	2	73.39
11992146	307.11	2.494166627	4	2	57.78
15602701	462.12	4.69320365	9	3	109.65

15991573	422.14	4.312930003	5	3	80.9
16040279	392.13	3.099456926	5	2	64.79
16122633	389.14	3.31420824	5	2	66.49
16752640	389.09	2.352833117	7	2	111.98
17758361	344.16	2.124410216	5	4	91.86
23658582	433.06	4.131804112	7	2	92.94
24764434	403.11	3.140948073	7	2	111.98
24812717	397.19	2.302565939	6	3	85.83
24832041	352.14	2.929404151	3	4	69.11
24864821	383.14	3.881028744	7	0	74.43
24875320	414.13	3.574844948	6	4	97.11
24882195	325.13	3.868303236	5	1	55.11
25023705	428.2	3.589120647	8	5	129.04
25134257	329.11	4.120637976	4	1	57.61

Table 6: Lipinski's Rule of five; Drug likeness of the compounds

Chapter 4. Discussion

The aim of this study was to use a multi-stage in silico screening pipeline to identify potential Tankyrase 1 (TNKS1) inhibitors from a library of 6,000 compounds obtained from DrugBank to disrupt Wnt/β-catenin signaling pathway, which is involved in the progression of ovarian cancer. These compounds were then narrowed down by performing a few successive steps of molecular docking, protein-ligand interaction analysis and ADMET profiling to identify a final set of lead candidates, with Ligand 16752640 emerging as the top hit, followed by Ligand 449087 and Tasosartan (Ligand 60919), both of which also demonstrated acceptable pharmacokinetic profiles.

The strict reference-derived cutoff (the docking scores of 3J5 and AZ6102, -13.8 and -13.2 kcal/mol respectively) proved too stringent when applied directly: only 2-3 compounds from the full 6,000-compound library possessed binding affinities more negative than these reference values. Such a small pool would not have provided sufficient candidates for the subsequent stages of interaction analysis and ADMET profiling. The selection criterion was therefore revised: rather than applying a fixed cutoff, the top 100 compounds with the most favorable binding affinity scores were shortlisted, preserving the conceptual link to reference inhibitor performance while yielding a practically screen able pool.

After the initial docking, the number of compounds was reduced further in two steps. The 100 compounds were first reduced to 60 through visual inspection in Discovery Studio, where each compound was evaluated to determine whether its binding pose was structurally reasonable. Second, based on how many of the same active-site amino acid residues (Ser1221, Gly1185, Tyr1213, Tyr1224, His1184, Ala1215, and Lys1220) these 60 compounds interacted with, they were compared to the two reference inhibitors, 3J5 and AZ6102. These residues are known to be crucial for TNKS1 inhibition. The list was reduced to 34 compounds by this comparison. This step was necessary because only a compound's docking score does not ensure that it works in a way that has biological significance. A compound is more likely to engage the target in a similar, functionally relevant way if it interacts with the same critical residues as known, active TNKS1 inhibitors, rather than simply scoring well by chance (Kitchen et al., 2004).

The best candidate was selected from 34 shortlisted compounds using the ADMET profiling. The 34 compounds were profiled for their ADMET properties to select the best candidate,

which turned out to be Ligand 16752640. This drug exhibited weak CYP2C9/CYP3A4 inhibitory activity, weak hERG inhibition (0.043), lowest plasma clearance among all the drugs (0.693) and negligible blood brain barrier penetration (0.00017). Based on these profiles, the overall profile of this compound is consistent with the ability to induce TNKS1-dependent Wnt/β-catenin signaling in ovarian cancer as a peripheral rather than central oncogenic pathway, with long half-life, low cardio toxic potential, and minimal potential for drug-drug interactions via CYP-mediated metabolism. Minimal BBB penetration is desirable here, since exposure to the CNS would cause unwanted neurological damage but not benefit the patient (Summerfield et al., 2014).

Ligand 16752640, with the IUPAC name 2-[(1R)-1-carboxy-2-naphthalen-1-ylethyl]-1,3-dioxoisoindole-5-carboxylic acid, is not an approved drug. According to PubChem & Drug Bank, it is an experimental compound which is classified as a member of the phthalimide chemical class, and was initially studied to bind to AmpC β-lactamase, a bacterial enzyme responsible for resistance to some antibiotics. Since this compound was not primarily designed or tested for cancer treatment, its appearance as the top candidate in this study raises the possibility of this molecule being a "drug repurposing" - a well-studied compound that may be given a completely new use, in this case, as an inhibitor for TNKS1 in the treatment of ovarian cancer.

The second-ranked candidate, Ligand 449087 (N-(3-cyclopropyl-1H-pyrazol-5-yl)-2-(2-naphthyl) acetamide), is a solid compound that contains a naphthalene group. It is known to target cyclin-A2 and cyclin-dependent kinase 2 (CDK2), two proteins that help to control cell division. Beyond just it’s docking and ADMET results, problems with CDK2 and cyclin-A2 are already linked to several cancers; this gives some extra biological evidence for this compound for being a good candidate. Finally, the third candidate, Tasosartan (Ligand 60919), is a long-acting drug that blocks angiotensin II receptors and is already used to treat high blood pressure. Unlike Ligand 16752640 and Ligand 449087, Tasosartan is already an approved drug. Therefore finding it here also points to a possible drug repurposing case, where a heart or blood pressure medicine could potentially be reused as a TNKS1 inhibitor for ovarian cancer.

However these results must be considered with the necessary degree of caution. As of today, none of the three candidates: Ligand 16752640, Ligand 449087, and Tasosartan (60919) has been experimentally tested against the TNKS1 or for any oncology-related assay. Their

identification here is based on computational prediction, but only this does not substitute for experimental confirmation. A handful of assays can be performed on these compounds, including in vitro enzymatic inhibition assays, cell-based Wnt/β-catenin reporter assays, and finally, in vivo efficacy studies in ovarian cancer models would be necessary to confirm their true TNKS1 inhibitory activity and antitumor efficacy.

Lastly, the identification of structurally diverse compounds from different therapeutic classes among the top candidates highlights the value of virtual screening in discovering potential drug repurposing opportunities that may not be identified through conventional oncology-focused approaches.

Chapter 5: Conclusion

In silico screening pipeline to identify potential Tankyrase 1 (TNKS1) inhibitors from a library of 6,000 compounds obtained from the DrugBank database was performed in this study using the PARP catalytic domain present in the 4W6E crystal structure. A series of binding affinity assays, protein-ligand interaction profiling against the reference inhibitors 3J5 and AZ6102, and in silico ADMET analysis successively reduced the number of candidates from 6,000 to one lead candidate. 100 most potential compounds were found by molecular docking based on their binding affinity. After visual inspection and interaction analysis against seven important residues in the active-site (Ser1221, Gly1185, Tyr1213, Tyr1224, His1184, Ala1215, Lys1220), 34 compounds were shortlisted that best mimicked the binding properties of the validated reference inhibitors. The 34 candidates were profiled by ADMET and Ligand 16752640 showed the lowest predicted plasma clearance (0.693 L/h/kg), minimal hERG inhibition (0.043), low Ames mutagenicity (0.210), negligible BBB penetration and acceptable CYP inhibition, while meeting all of Lipinski's Rule of Five. All of these properties suggest good oral bioavailability, low cardiac and hepatic toxicity risk, and a favorable pharmacokinetic profile for a peripherally acting anticancer drug for ovarian cancer. The results demonstrate that structure-based virtual screening of TNKS1 as a viable approach to discover drug-repurposing candidates for the Wnt/β-catenin pathway inhibitory activity in ovarian cancer. The potential of the compound, Ligand 16752640, to inhibit TNKS1 action and its therapeutic implications should be further confirmed by molecular dynamics simulation, binding free energy calculation and experimental testing in ovarian cancer cell lines overexpressing TNKS1.

References

Bilbao-Aldaiturriaga, N., Martínez-Agüero, A., García-Orad, A., & Patino-Garcia, A. (2021). Tankyrases as modulators of pro-tumoral functions: Molecular insights and therapeutic opportunities. *Journal of Experimental & Clinical Cancer Research, 40,* 144. https://doi.org/10.1186/s13046-021-01950-6

Li, R., Zhao, A., Liu, M., Lu, L., Li, B., & Zeng, H. (2026). Global epidemiology of ovarian cancer: Patterns, trends, and risk factors. *Cancer Biology & Medicine*. Advance online publication. https://doi.org/10.20892/j.issn.2095-3941.2025.0619

Fahad Al Qooz, Mohammad Alanazi, Mohammad S. Al Olaimat, Tasneem Malahmeh, & Zaid Rasheed Alzoubi. (2024). Submandibular basal cell adenoma - A rare presentation. *Human Pathology Reports, 35,* Article 300729.

Huang, S.-M. A., Mishina, Y. M., Liu, S., Cheung, A., Stegmeier, F., Michaud, G. A., Charlat, O., Wiellette, E., Zhang, Y., Wiessner, S., Hild, M., Shi, X., Wilson, C. J., Mickanin, C., Myer, V., Fazal, A., Tomlinson, R., Serluca, F., Shao, W., … Cong, F. (2009). Tankyrase inhibition stabilizes axin and antagonizes Wnt signalling. *Nature, 461(7264),* 614–620. https://doi.org/10.1038/nature08356

Kurman, R. J., & Shih, I.-M. (2016). The dualistic model of ovarian carcinogenesis: Revisited, revised, and expanded. *American Journal of Pathology, 186(4),* 733–747. https://doi.org/10.1016/j.ajpath.2015.11.011

Lin, K. Y., Way, T. D., Lai, C. H., & Cheng, H. C. (2019). Tankyrase promotes aerobic glycolysis and proliferation of ovarian cancer through activation of Wnt/β-catenin signaling. *BioMed Research International, 2019,* Article 2686746. https://doi.org/10.1155/2019/268634

Li, B., Liang, J., Lu, F., Zeng, G., Zhang, J., Ma, Y., Liu, P., Wang, Q., Zhou, Q., & Chen, L. (2020). Discovery of Novel Inhibitor for WNT/β-Catenin Pathway by Tankyrase 1/2 Structure-Based Virtual Screening. *Molecules, 25(7),* 1680. https://doi.org/10.3390/molecules25071680

Sciallis, A., & Zhang, G. (2024). Epithelial tumors of the ovary: A review focusing on carcinoma and recent advances. *Human Pathology Reports, 37,* 300749. https://doi.org/10.1016/j.hpr.2024.300749

Berishvili, V. P., Kuimov, A. N., Voronkov, A. E., Radchenko, E. V., Kumar, P., Choonara, Y. E., Pillay, V., Kamal, A., & Palyulin, V. A. (2020). Discovery of Novel Tankyrase Inhibitors through Molecular Docking-Based Virtual Screening and Molecular Dynamics Simulation Studies. *Molecules, 25(14),* 3171. https://doi.org/10.3390/molecules25143171

Riccio, A. A., McCauley, M., Langelier, M.-F., & Pascal, J. M. (2016). Tankyrase requires SAM domain-dependent polymerization to support Wnt-β-catenin signaling. *Molecular Cell, 63(3),* 497–510. https://doi.org/10.1016/j.molcel.2016.06.020

World Cancer Research Fund International. (2025). *Ovarian cancer statistics.* https://www.wcrf.org/preventing-cancer/cancer-statistics/ovarian-cancer-statistics/

Helen M. Berman, John Westbrook, Zukang Feng, Gary Gilliland, T. N. Bhat, Helge Weissig, Ilya N. Shindyalov, Philip E. Bourne, The Protein Data Bank, *Nucleic Acids Research,* Volume 28, Issue 1, 1 January 2000, Pages 235–242, https://doi.org/10.1093/nar/28.1.235

David S Wishart, Yannick D Feunang, An C Guo, Elvis J Lo, Ana Marcu, Jason R Grant, Tanvir Sajed, Daniel Johnson, Carin Li, Zinat Sayeeda, Nazanin Assempour, Ithayavani Iynkkaran, Yifeng Liu, Adam Maciejewski, Nicola Gale, Alex Wilson, Lucy Chin, Ryan Cummings, Diana Le, Allison Pon, Craig Knox, Michael Wilson, DrugBank 5.0: a major update to the DrugBank database for 2018, *Nucleic Acids Research,* Volume 46, Issue D1, 4 January 2018, Pages D1074–D1082, https://doi.org/10.1093/nar/gkx1037

Sunghwan Kim, Jie Chen, Tiejun Cheng, Asta Gindulyte, Jia He, Siqian He, Qingliang Li, Benjamin A Shoemaker, Paul A Thiessen, Bo Yu, Leonid Zaslavsky, Jian Zhang, Evan E Bolton, PubChem 2019 update: improved access to chemical data, *Nucleic Acids Research,* Volume 47, Issue D1, 08 January 2019, Pages D1102–D1109, https://doi.org/10.1093/nar/gky1033

The PyMOL Molecular Graphics System, Version 2.0. Schrödinger, LLC.

Morris, G.M., Huey, R., Lindstrom, W., Sanner, M.F., Belew, R.K., Goodsell, D.S. and Olson, A.J. (2009), AutoDock4 and AutoDockTools4: Automated docking with selective receptor flexibility. *J. Comput. Chem*., 30: 2785-2791. https://doi.org/10.1002/jcc.21256

O'Boyle, N.M., Banck, M., James, C.A. et al. Open Babel: An open chemical toolbox. *J Cheminform* 3, 33 (2011). https://doi.org/10.1186/1758-2946-3-33

Trott, O. & Olson, A. J. (2010). AutoDock Vina. Journal of Computational Chemistry, 31(2), 455–461. Trott, O. and Olson, A.J. (2010), AutoDock Vina: Improving the speed and accuracy of docking with a new scoring function, efficient optimization, and multithreading. *J. Comput. Chem.*, 31: 455-461. https://doi.org/10.1002/jcc.21334

BIOVIA Discovery Studio Visualizer, v21.1.0. Dassault Systèmes, San Diego, 2021.

Bijani, S., Iqbal, D., Mirza, S., Jain, V., Jahan, S., Alsaweed, M., Madkhali, Y., Alsagaby, S. A., Banawas, S., Algarni, A., Alrumaihi, F., Rawal, R. M., Alturaiki, W., & Shah, A. (2022). Green Synthesis and Anticancer Potential of 1,4-Dihydropyridines-Based Triazole Derivatives: In Silico and In Vitro Study. *Life*, 12(4), 519. https://doi.org/10.3390/life12040519

Kennedy, T. (1997). Managing the drug discovery/development interface. *Drug Discovery Today*, 2(10), 436–444. https://doi.org/10.1016/S1359-6446(97)01099-4

Johannes JW, Almeida L, Barlaam B, Boriack-Sjodin PA, Casella R, Croft RA, Dishington AP, et al. (2015). Pyrimidinone nicotinamide mimetics as selective tankyrase and Wnt pathway inhibitors suitable for in vivo pharmacology. *ACS Medicinal Chemistry Letters*, 6(3), 254–259. https://doi.org/10.1021/ml5003663

Veber, D. F., Johnson, S. R., Cheng, H.-Y., Smith, B. R., Ward, K. W., & Kopple, K. D. (2002). Molecular properties that influence the oral bioavailability of drug candidates. *Journal of Medicinal Chemistry*, 45(12), 2615–2623. https://doi.org/10.1021/jm020017n

Lipinski, C. A., Lombardo, F., Dominy, B. W., & Feeney, P. J. (1997). Experimental and computational approaches to estimate solubility and permeability in drug discovery and development settings. *Advanced Drug Delivery Reviews*, 23(1–3), 3–25. https://doi.org/10.1016/S0169-409X(96)00423-1

Li Fu, Shaohua Shi, Jiacai Yi, Ningning Wang, Yuanhang He, Zhenxing Wu, Jinfu Peng, Youchao Deng, Wenxuan Wang, Chengkun Wu, Aiping Lyu, Xiangxiang Zeng, Wentao Zhao, Tingjun Hou, Dongsheng Cao, ADMETlab 3.0: an updated comprehensive online ADMET prediction platform enhanced with broader coverage, improved performance, API functionality

and decision support, *Nucleic Acids Research*, Volume 52, Issue W1, 5 July 2024, Pages W422–W431, https://doi.org/10.1093/nar/gkae236

Di, L., & Kerns, E. H. (2010). Drug-like Properties: Concepts, Structure Design and Methods: from ADME to Toxicity Optimization. *Elsevier*.

Artursson, P., & Karlsson, J. (1991). Correlation between oral drug absorption in humans and apparent drug permeability coefficients in human intestinal epithelial (Caco-2) cells. *Biochemical and Biophysical Research Communications, 175*(3), 880–885.

Di, L., Kerns, E. H., Fan, K., McConnell, O. J., & Carter, G. T. (2003). High throughput artificial membrane permeability assay for blood-brain barrier. *European Journal of Medicinal Chemistry, 38*(3), 223–232.

Summerfield, S. G., Stevens, A. J., Cutler, L., Del Carmen Osuna, M., Hammond, B., Tang, S. P., Hersey, A., Spalding, D. J., Jeffrey, P., & Redfern, W. S. (2014). Restricting CNS penetration of drugs to minimise adverse events: Role of drug transporters. *Drug Discovery Today: Technologies, 12*, e79–e85. https://doi.org/10.1016/j.ddtec.2014.03.008

Zanger, U. M., & Schwab, M. (2013). *Cytochrome P450 enzymes in drug metabolism: Regulation of gene expression, enzyme activities, and impact of genetic variation*. *Pharmacology & Therapeutics, 138*(1), 103–141. https://doi.org/10.1016/j.pharmthera.2012.12.007

Guengerich, F. P. (2008). Cytochrome P450 and chemical toxicology. *Chemical Research in Toxicology, 21*(1), 70–83.

Obach, R. S., Lombardo, F., & Waters, N. J. (2008). Trend analysis of a database of intravenous pharmacokinetic parameters in humans for 670 drug compounds. *Drug Metabolism and Disposition, 36*(7), 1385–1405. https://doi.org/10.1124/dmd.108.020479

Di, L., & Kerns, E. H. (2009). Application of drug-like property concepts in pharmaceutical design. *Current Pharmaceutical Design, 15*(19), 2184–2194.

Mortelmans, K., & Zeiger, E. (2000). *The Ames Salmonella/microsome mutagenicity assay*. *Mutation Research/Fundamental and Molecular Mechanisms of Mutagenesis*, *455*(1–2), 29–60. https://doi.org/10.1016/S0027-5107(00)00064-6

Chen, M., Borlak, J., & Tong, W. (2013). High lipophilicity and high daily dose of oral medications are associated with significant risk for drug-induced liver injury. *Hepatology*, *58*(1), 388–396.

Vinken, M. (2015). Adverse outcome pathways and drug-induced liver injury testing. *Chemical Research in Toxicology*, *28*(8), 1391–1397.

Sanguinetti, M. C., & Tristani-Firouzi, M. (2006). hERG potassium channels and cardiac arrhythmia. *Nature*, *440*(7083), 463–469. https://doi.org/10.1038/nature04710

Redfern, W. S., Carlsson, L., Davis, A. S., Lynch, W. G., MacKenzie, I., Palethorpe, S., Siegl, P. K. S., Strang, I., Sullivan, A. T., Wallis, R., Camm, A. J., & Hammond, T. G. (2003). Relationships between preclinical cardiac electrophysiology, clinical QT interval prolongation and torsade de pointes for a broad range of drugs: Evidence for a provisional safety margin in drug development. *Cardiovascular Research*, *58*(1), 32–45. https://doi.org/10.1016/S0008-6363(02)00846-5

Raschi, E., Ceccarini, L., De Ponti, F., & Recanatini, M. (2009). hERG-related drug toxicity and models for predicting hERG liability and QT prolongation. *Expert Opinion on Drug Metabolism & Toxicology*, *5*(9), 1005–1021. https://doi.org/10.1517/17425250903049875

Kitchen, D., Decornez, H., Furr, J. *et al.* Docking and scoring in virtual screening for drug discovery: methods and applications. *Nat Rev Drug Discov* 3, 935–949 (2004). https://doi.org/10.1038/nrd1549

Project Writeup

ORIGINALITY REPORT

5%	3%	2%	2%
SIMILARITY INDEX	INTERNET SOURCES	PUBLICATIONS	STUDENT PAPERS

PRIMARY SOURCES

1	Submitted to University of Bedfordshire Student Paper	
2	ligand-depot.rutgers.edu Internet Source	
3	Mingfeng Yu, Yuchao Yang, Matthew Sykes, Shudong Wang. "Small-Molecule Inhibitors Tankyrases as Prospective Therapeutics for Cancer", Journal of Medicinal Chemistry, 20 Publication	
4	icb13.znu.ac.ir Internet Source	
5	0-www.ncbi.nlm.nih.gov.linyanti.ub.bw Internet Source	

Exclude quotes	Off	Exclude matches < 1%
Exclude bibliography	On	